VILNIUS UNIVERSITY

SIMONA STEPONKIENE

THE EFFECT OF NANOCOMPOSITES ON CANCER STEM CELLS

Summary of doctoral dissertation
Biomedical sciences, biophysics (02 B)

Vilnius, 2014

The study was carried out in Vilnius University during the period 2010 – 2014.

The experiments were carried out in the Biomedical Physics Laboratory of the Institute of Oncology, Vilnius University and in the Institute of cancer research, Oslo university hospital.

Scientific supervisor:

Prof. habil. dr. Ricardas Rotomskis (Vilnius University, biomedical sciences, biophysics – 02B)

Doctoral dissertation will be defended at the Council of Scientific Field of Biophysics of Vilnius University:

Chairman:

Prof. dr. Aidas Alaburda (Vilnius University, Biomedical sciences, Biophysics – 02B)

Members:

Doc. dr. Almira Ramanaviciene (Vilnius University, Biomedical sciences, Biology – 01B)

Prof. habil. dr. Vytenis Arvydas Skeberdis (Lithuanian University of Health sciences, Biomedical sciences, Biophysics – 02B)

Dr. Augustas Pivoriunas (Center of Innovative Medicine, Physical sciences, Biochemistry – 04P)

Dr. Asta Juzeniene (Institute of cancer research, Oslo University Hospital, Biomedical sciences, Biophysics – 02B)

Dissertation will be defended during an open session of the Council of Scientific Field of Biophysics on 30th of September, 2014 at 16:00 in the Biophysics Auditorium (242), Faculty of Natural Sciences of Vilnius University.
Address: M. K. Ciurlionio st. 21/27, LT – 03101, Vilnius, Lithuania

Summary of doctoral dissertation was disseminated on 28th of August, 2014.
Doctoral dissertation is available at the library of Vilnius University.

VILNIAUS UNIVERSITETAS

SIMONA STEPONKIENĖ

NANODARINIŲ POVEIKIO VĖŽINĖMS KAMIENINĖMS LĄSTELĖMS TYRIMAS

Daktaro disertacija

Biomedicinos mokslai, biofizika (02B)

Vilnius, 2014

Disertacija rengta 2010 – 2014 metais Vilniaus universitete

Eksperimentiniai darbai atlikti Vilniaus universiteto Onkologijos institute ir Oslo universitetinės ligoninės Vėžio tyrimų insititute

Mokslinis vadovas:
Prof. habil. dr. Ričardas Rotomskis (Vilniaus universitetas, biomedicinos mokslai, biofizika – 02 B)

Disertacija ginama Vilniaus universiteto Biofizikos mokslo krypties taryboje:
Pirmininkas – prof. dr. Aidas Alaburda (Vilniaus universitetas, biomedicinos mokslai, biofizika – 02B).
Nariai:
Doc. dr. Almira Ramanavičienė (Vilniaus universitetas, biomedicinos mokslai, biologija – 01B)
Habil.dr. Vytenis Arvydas Skeberdis (Lietuvos sveikatos mokslų universitetas, biomedicinos mokslai, biofizika – 02B) .
Dr. Augustas Pivoriūnas (Vilniaus universitetas, fiziniai mokslai, biochemija – 04P)
Dr. Asta Juzėnienė (RadiumHospitalet, Oslo universitetinė ligoninė, biomedicinos mokslai, biofizika – 02B)

Disertacija bus ginama viešame Biofizikos mokslo krypties tarybos posėdyje 2014 m. Rugsėjo mėn. 30 d. 16:00 val. Gamtos mokslų fakulteto Biofizikos (242) auditorijoje. Adresas: M. K. Čiurlionio 21/27, LT – 03101, Vilnius, Lietuva.

Disertacijos santrauka išsiuntinėta 2013 m. rugpjūčio mėn. 28 d.

Disertaciją galima peržiūrėti Vilniaus universiteto bibliotekoje.

Table of Contents

ABBREVIATIONS

CSC – cancer stem cells

QD – quantum dots

CdTe-MPA – quantum dots composed of CdTe and mercaptopropionic acid

RPMI –Growth medium of Roswell Park Memorial Institute for cell culturing

DMEM - Dulbecco's modified Eagle's medium for cell culturing

DPBS – Dulbecco phosphate buffered saline (pH 7.4), supplemented with Ca^{2+} ir Mg^{2+};

PBS - phosphate buffered saline, pH 7.4

MEM – *Minimal essential medium*for cell culturing

EDTA – Ethylenediaminetetraacetic acid

XTT – 2,3-Bis-(2-Methoxy-4-Nitro-5-Sulfophenyl)-2H-Tetrazolium-5-Carboxanilide

FITC – Fluorescein isothiocyanate – a fluorochrome for immunofluorescence staining

PE – Phycoerythrin – a fluorochrome for immunofluorescence staining

Anti-CD44 – antibody against CD44 surface protein

Anti-CD133 – antibody against CD133 surface protein

RGB – 3 channel (red, green, blue) detection system

NP – nanoparticle

PL – photoluminescence

FRET – Fiorster resonance energy transfer

PDT – photodynamic therapy

PS – photosensitizer

Ce_6 – photosensitizer chlorin e_6

PEG – polietilenglicol

AMP – amphiphilic polymer

AML – amphiphilic lipid

1. INTRODUCTION

Recent advances in cancer research offers well developed pharmaceutics and novel cure strategies. Hower, recurrence of oncological deseases after treatment still remains as a huge issue. According to statistics of the World Cancer Research, 14 millions of cancer patients were registered in 2012 and this number is prognosed to increase to 24 millions in 2035 [1]. Emerging evidence has shown that the capacity of a tumor to grow and propagate is dependent on a small subset of cells, termed “cancer stem cells“ [2]. Conventional treatments, however, may miss the cancer stem cells, which have been shown in several tumor types to be more resistant to standard chemotherapeutic agents, because the cancer stem cell survives and regenerates the neoplasm [3, 4]. Tumor metastasis are also associated with the migratory capacity of cancer stem cells [5]. Increasing number of publication in the field of targeted therapy propose the CSCs to be the main target in anti-cancer therapies. Identification and eradication of CSCs could lead to more effective and selective treatment of oncological deseases and thus avoid tumor progression, recurrence and metastasis.

Rapid development of nanotechnologies has already resulted in creation of novel therapeutics. The unique chemical and physical properties of nanoparticles and nanocomposites led to application of these new agents in the experimental oncology [6].Therefore it is important to continue development of nanotechnologies and to focus on CSC-adressed noninvasive diagnostics and treatment of cancer. Primary studies on CSC eradication by nanoparticle-based thermolysis has already been performed [7, 8]. The CSC directed selective killing was successfully achieved. These promising results of these studies encourage for the investigation of theranostic agents, combining capability of diagnostic as well as killing of CSCs.

1.1. The aim of the study and objectives

The aim:

To investigate the applicability of quantum dots in CSC detection and eradication.

Objectives:

1) To investigate the accumulation of CdTe-MPA in melanoma stem cells;
2) To compare the accumulation and toxicity of CdTe-MPA and CdSe/ZnS-(AMP)-COOH QDs in human cancer cells;
3) To investigate the localization of CdSe/ZnS-(AML/PEG)-COOH QDs and anti-CD44-FITC conjugate in human breast cancer stem cells;
4) To investigate the cellular uptake, energy transfer and photosensitizing properties of the CdSe/ZnS-(AML/PEG)-COOHQDs and photosensitizer Ce_6 nanocomposite *in vitro*;
5) To measure the stability of non-covalent CdSe/ZnS-(AML/PEG)-COOH QDs and photosensitizer Ce_6 complex in the cell growth medium, thus simulating *in vivo* blood system.

1.2. Defended statements

1) $CD44^{high}CD133^{low/-}$ subpopulation of FEMX-I melanoma cells possess properties of cancer stem cells.

2) CdTe-MPA and CdSe/ZnS-(AMP)-COOH QDs accumulate in all types of human cancer cells in a concentration-dependant way and localize inside cells in the vesicular structures near nucleus.

3) Due to higher PL intensity and non-toxic behaviour, CdSe/ZnS-(AMP)-COOH QDs are more suitable for application of nanocomposites in the imaging of cancer stem cells.

4) Conjugates of CdSe/ZnS-(AML/PEG)-COOH QDs and anti-CD44 are packed into vesicles selectively inside $CD44^+$ cells, while anti-CD44-FITC conjugates remain on the plasma membrane.

5) The complex of CdSe/ZnS-(AML/PEG)-COOH QDs and photosensitizer chlorin e_6 accumulates inside plasma membrane and vesicles of cancer cells, and initiates light-mediated cell death via energy transfer from QDs to Ce_6 molecules.

6) When incubation of the non-covalent CdSe/ZnS-(AML/PEG)-COOH-Ce_6 complex is conducted in culture medium vs physiological saline, better stability and energy transfer is registered inside cells.

1.3. Scientific novelty and actuality

Despite these numerous advances in the treatment of metastatic disease, responses to the existing conventional treatment have not been consistent, predictable or durable in many cases. A topic of growing interest that may generate new insights into the pathogenesis of cancer reccurence and metastasis is the emerging cancer stem cell field. CSCs are tumor subpopulations in which clinical virulence resides as a consequence of their unlimited capacity to proliferate, self-renew and differentiate into more mature tumor populations to sustain robust tumor progression [9-11]. Increasing evidences support the idea that, instead of merely targeting the bulk non-CSCs, successful cancer curing may require both undifferentiated CSCs and differentiated non-CSCs to be efficiently eliminated. Scientists are working on identification of molecular markers, which could selectively detect the „most dangerous“ cells and eliminate their population thus stopping the progression of the deasease as well as metastasis. Numerous number of markers have been already reported for different types of cancer [12-14]. However it is still under consideration whether such markers are capable of labelling a whole population of CSCs [15]. Therefore, despite immunophenotyping, the capabilty of tumour formation, migration and resistance to chemo- and radiotherapies are performed in order to characterise CSCs completely.

Advances in nanotechnology have contributed to the development of novel nanoparticles that enable the tumor-specific delivery of imaging probes and therapeutic agents in cancer imaging and therapy. Nanobiotechnology combines nanotechnology with molecular imaging, which has led to the generation of new multifunctional nanoparticles for cancer imaging and therapy. Multifunctional nanoparticles hold great promise for the future of cancer treatment because they can detect the early onset of cancer in each individual patient and deliver suitable therapeutic agents to enhance therapeutic efficacy. The combination of tumor-targeted imaging and therapy in an all-in-one system provides a useful multimodal approach in the battle against cancer [16]. QDs have gained much attetion due to unique optical and electronic properties, such as size- and composition-tunable fluorescence emission from visible to infrared wavelengths, large absorption coefficients across a wide spectral range and very high levels of brightness and photostability [17, 18]. Easy surface chemistry of QDs allows

conjugation of the bioactive molecules (antibodies, etc.) and various therapy agents – chemotherapeutic drug or photosensitizer [19, 20]. Peptide- and antibodies-coated QDs have already been reported to selectively detect cancer cells *in vivo*[21, 22]. However the information about usage of QDs in CSC detection and treatment is still missing.

The combination of semiconductor quantum dots with PDT photosensitizers enables the use of an excitation wavelength where the photosensitizer alone does not absorb [23]. Since quantum dots exhibit broad absorption spectra, their conjugation to a PDT photosensitizer provides flexibility to utilize variable excitation wavelengths to activate the photosensitizer molecule and thus to innitiate sigulet oxygen-mediated death of cancer cells. First studies on QD-PS nanocomposites showed energy transfer from QDs and PSs as well as production of reactives oxygen species[24, 25]. However, the knowledge about QD-PS biocompatibility, accumulation in cancer cells and photosensitizing properties are still missing.

In this work for the first time the sensitivity of FEMX-I melanoma cells to ionizing radiation was shown. Also it has been documented that despite phenotypical and funcional diversity all cells are capable of QDs accumulation. Additionally, it has been shown for the first time that anti-CD44-QDs conjugates accumulate selectively inside $CD44^+$ cells and localize in the endocytic vesicles, while anti-CD44-FITC is not capable of entering inside cells. Moreover the complex of QDs and photosensitizer chlorin e_6 accumulates inside cells and innitiates light-mediated cell death via energy transfer from QDs to Ce_6 molecules.These results show the capability of quantum dots to selectively diagnose and treat cancer. In the future studies the capacity of selective recognision and therapy will be combined thus creating a novel multifuncional theranostic agent.

2. MATERIALS AND METHODS

2.1. Materials

A pancreatic adenocarcinoma (MiaPaCa2) cell line was purchased from the Health Protection Agency Culture Collections. Prostate adenocarcinoma (PC3) and glioblastoma (U87) cells were obtained from the American Type Culture Collection. Melanoma (FEMX-I) cells were originally derived from lymph node metastasis of a patient with melanoma at the Norwegian Radiumhospital in 1980 [26]. Human breast cancer cell lines MDA-MB-231 and MCF-7 were obtained from the American Type Culture Collection (ATCC). CdTe QDs coated with mercaptopropionic acid (MPA) were purchased from PlasmaChem GmbH (Berlin, Germany) emitting far-red fluorescence (λ_{max} = 710 ± 5 nm). Commercial carboxyl-Functionalized eFluor® 605NC QDs, composed of CdSe/ZnS core/shell, outer lipid coating with polyethylene glycol and carboxyl functional groups, were purchased from eBioscience (USA). Commercial carboxyl-Functionalized eFluor® 605NC anti-CD44-QD conjugate, composed of CdSe/ZnS core/shell, outer lipid coating with polyethylene glycol and carboxyl functional groups as well as antibodies agains CD44 antigen, were purchased from eBioscience (USA). Ce_6 was obtained from Frontier Scientific Inc. (USA).

2.2. Cell culturing

Cells were cultured in DMEM or RPMI. Both growth mediums contained 10% fetal bovine serum (FBS, Fisher Scientific, Oslo, Norway), 100 U/ml penicillin, 100 mg/ml streptomycin, and 2 mM L-Glutamine (Sigma-Aldrich Norway AS, Oslo, Norway). In the case of the U87 cells, the DMEM medium was additionally supplemented with 3% MEM non-essential amino acids (Sigma-Aldrich). The cells were routinely cultivated in 25 cm^2 Nunclon culture dishes (VWR International, Oslo, Norway) under standard conditions, subculturing them twice a week and keeping them in a humidified incubator at 37°C with 5% CO_2. For experiments, the cells were harvested by bringing them into suspension via trypsinization and seeding a necessary amount of cells into multiplates.

2.3. Assessment of CSC properties

For the assessment of the expression of stem-like surface antigens up to 10^6 cells were labeled in PBS solution with anti-CD44-FITC (BD Biosciences, USA), anti-CD133-PE (eBioscience, USA) for 20 min at room temperature. Flow cytometric analysis was carried out with a FACSort or LSR II analyzer (BD Biosciences). The data were analyzed with FlowJo (Tree Star, USA) software. A minimum of 10,000 viable cells were measured per sample. Using forward and side scatter profiles and propidium iodide (PI) staining, debris, cell doublets, and dead cells were gated out, respectively. Fluorescence-activated cell sorting was performed on a BD FACSAria or FACSort Cell Sorter (BD Biosciences). Purities of the sorted populations, as determined by post-sorting flow analysis, were generally >90%.

To determine the sensitivity of FEMX-I cells to the treatment of ionizing radiation, cells were seeded into multiplates and kept for 24 hours. Cells were exposed to different doses of ionizing radiation ranging from 0 to 10 Gy delivered by a Müller X-ray apparatus operated at 220 kV, 20 mA, with a 0.5 mm Cu filter (Oslo university hospital, Norway). After 24 hours the immunophenotyping by using anti-CD44-FITC and anti-CD133-PE was performed.

2.4. Cellular uptake of CdTe-MPA QDs in cancer cells

A stock solution of CdTe-MPA QDs was prepared by dissolving 1 mg QDs in 1 ml PBS (Sigma-Aldrich) at pH 7.4 or saline (0.9% w/v NaCl). The stock solution was further diluted to a desired concentration in DMEM or RPMI-1640 growth medium and poured over the FEMX-I cells growing in the multiplates. The medium without QDs was poured in a few wells to have control cells in the same multiplate. After incubation at 37°C for 24 h, the cells were washed with ice-cold PBS+ (standard PBS supplemented with 0.9 mM $CaCl_2$ and 0.5 mM $MgCl_2$ to prevent cell detachment at this step) to remove any free QDs. Immediately after washing, the cells were brought into suspension by trypsinization for further analysis using flow cytometry.

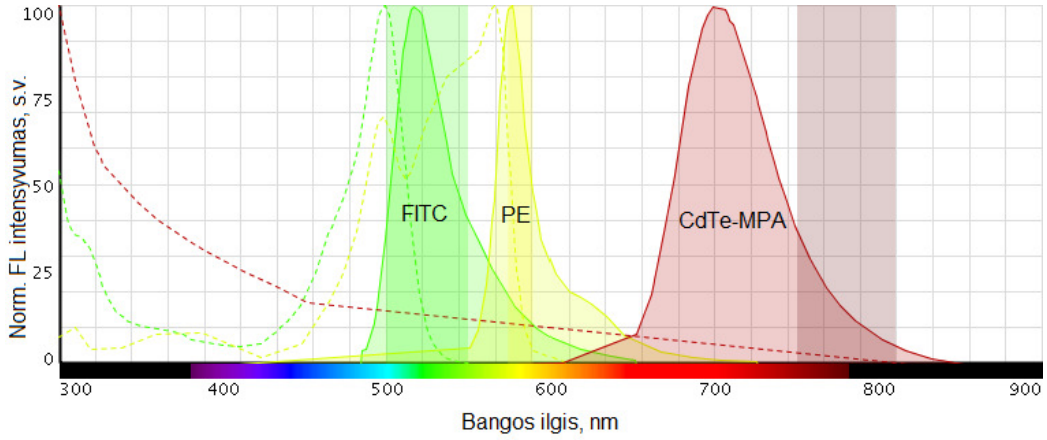

Fig. 2.4.1. Bandpass filters of *BD™ LSR II* flow cytometer, marked as green, yellow and violet rectangle. The emission and exitation of fluorescent agents of FITC, PE and CdTe-MPA are marked as a line and a dotted line respectively.

2.5. UV-VIS and time-resolved spectroscopy of QDs and chlorin e_6 complex

The steady state absorption and the fluorescence spectra of samples were recorded with a Cary 50 UV-Vis absorption (Varian, Inc., USA) and a Cary Eclipse fluorescence spectrometers (Varian, Inc., USA), respectively. Fluorescence decay measurements were performed with F920 spectrometer (Edinburgh Instruments, UK), equipped with a single photon photomultiplier detector (S900-R) [27]. The excitation source was a picosecond pulsed diode laser (EPL-405) with a radiation wavelength at 405 nm. Quartz cuvettes with the optical path length of 1 cm were used for measurements. PL decays were analyzed by approximation with 3-exponential funcion. The avarge lifetime of PL was calculated as [27]:

$$< \tau >= \frac{\sum_i B_i {\tau_i}^2}{\sum_i B_i \tau_i}$$

τ_i – avarage lifetime, B_i – the aplitude of the component (t = 0), i – number of the component.

2.6. Intracellular distribution of QD-Ce_6 complex and energy transfer from QDs to Ce_6 in live cancer cells

For intracellular imaging studies, cells were seeded into 8-chambered cover glass plate (Nalge Nunc International, USA). $3x10^4$ cells were seeded into each chamber and incubated with QDs (0.2 μM), Ce_6 (1 μM) and QD-Ce_6 (molar ratio 1:5) complex in DPBS. After 3 h incubation the old medium was carefully aspirated, the cells were washed twice with DPBS and supplemented with fresh DPBS. The cellular uptake of QD-Ce_6 complex was assessed using Nikon Eclipse Te2000-U microscope with Confocal Laser Scanning system C1si equipped with CO_2 Microscope Stage Incubation System (OkoLab, Italy). For precise measurements, emission of QDs and Ce_6 was separated using microscope spectral imaging unit (capable of 32 bit spectral imaging). A desired spectral range (580-730 nm) was recorded with 32 channels, 16 channels were assigned to spectral range of QDs emission (580-655 nm – "a green image") and the rest were assigned to Ce_6 emission (656-730 nm – "a red image") using 5 nm step of spectral measurement. Measurements were done using 60x/1.4 NA oil immersion objective and 488 nm argon-ion laser. The data were analysed using EZ-C1 3.80 FreeViewer (Nikon) and ImageJ (De Novo Software).

For confirmation of FRET inside live cancer cells, the fluorescence lifetime imaging microscopy was performed. Cells were prepared for the experiment as described previously, lifetime imaging was done using Lifetime and FCS Upgrade for Nikon C1si (PicoQuant GmbH, Germany). The system consisted of a 404 nm pulse diode laser with a pulse width of 39 ps and repetition rate of 10 MHz. Fluorescence signal was filtered by a band-pass 578±52.5 nm filter. Detected photons were counted by a time correlated single-photon counter PicoHarp 300 (PicoQuant GmbH, Germany). Initialization, scanning, and acquisition were controlled by the same Nikon C1si microscope system. FRET images were reconstructed using three exponential fitting model (SymPhoTime software, PicoQuant GmbH, Germany), in which average lifetime of a fluorescent agent is displayed for every given pixel. Histograms for all average lifetimes (for all pixels) of QDs and QD-Ce_6 complex were plotted using the same SymPhoTime software.

2.7. Photosensitizing properties of QD-Ce_6 complex

Photosensitizing properties was measured as a capability of QD-Ce_6 complex to induce obvious cell death via QD-directed irradiation. Cells were seeded for the experiment as described previously. After 24 hours the medium was replaced with 300 µl DPBS containing QDs (0.01 µM), Ce6 (0.05 µM), QD-Ce_6 (molar ratio 1:5) complex in DPBS and left for 3 hours in the incubator (in the dark). For irradiation procedure, cells were transferred to Microscope Stage Incubation System (OkoLab, Italy). The cells were irradiated with blue light (470±5 nm) using light source MAX-302 (Asahi Spectra CO., Ltd, Japan) with an in-built narrow band-pass filter. The light intensity measured at the sample position was 33 mW/cm^2. Irradiation was applied for 9 minutes for each well, giving a dose of 17.7 J/cm^2.

The viability was measured 20 hours after irradiation by adding 5 µl (100 µg/ml) of propidium iodide into each well and registering both fluorescence and bright field microscopy images. Statistical significance was counted using Student T-test by MS Excel program. $P<0.05$ were considered to be statistically significant.

2.8. Accumulation of anti-CD44-QD in MCF-7 and MDA-MB-231 cancer cells

QDs were diluted to a concentration of 5×10^{-8} M in the complete growth medium and poured over the MCF-7 and MDA-MB-231 cells growing in the 8-well glass chamber slide. After the desired time of incubation at 37°C the cells were washed with Dulbecco's PBS (supplemented with Ca^{2+} and Mg^{2+} to prevent cell detachment) (Biochrom, Germany) to remove any excess QDs and were fixed with 4% PFA (Sigma-Aldrich, Germany) for 15 min, permeabilized for 4 min using 0.2% Triton X-100 (Sigma-Aldrich, Germany) and blocked for 20 min with PBS containing 1% BSA (Sigma-Aldrich, Germany). To label actin, fixed and BSA-blocked cells were incubated with phalloidin- Alexa Fluor® 488 (Life Technologies, USA) methanolic solution for 20 min. To label nuclei, both fixed and live cells were incubated with 25 µg/ml Hoechst 33258 (Sigma-Aldrich, Germany) for 30 min. After staining cells were mounted on slides using Qdot® Mounting media (Life Technologies, USA) with coverslips. Labeling of actin and nuclei was made after the incubation with QDs.

For selective labelling studies, MCF-7 and MDA-MB-231 cells were set into 8-chambered plates. After 24 hours the medium was aspirated, 100 µl of DPBS solution containing 20 µL of anti-CD44-QDs and anti-CD44-FITC were poured over the cells for 30min. Live cell imaging was performed at two points of time: immediatelly after labelling and 24 hours after labelling.

Samples were examined under confocal microscope by scanning with the beam of UV laser (404 nm) for Hoechst, argon ion laser (488 nm) for phalloidin and FITC, and helium-neon laser (543 nm) for QDs using oil immersion 60x NA 1.4 objective (Plan Apo VC, Nikon, Japan). Images were captured and processed with EZ-C1 3.90 image analysis software (Nikon Instruments, USA).

3. RESULTS AND DISCUSSION

3.1. Identification of CSC

Heterogeneity of four cancer cell lines using putative stem cell markers for CD133 and CD44 was investigated. The cell-surface associated CD44 is an adhesion glycoprotein. The function of CD133 is still unknown, but it has been shown to be involved in dynamics of membrane protrusions and to mark cancer stem cells. The flow cytometry technique was performed to detect fluorescence from single cell after combined staining with antibody-dye conjugates against CD133 and CD44. All cell lines expressed CD44 to a similar degree, from 96.2 to 99.9% (Fig. 3.1.1). However, the

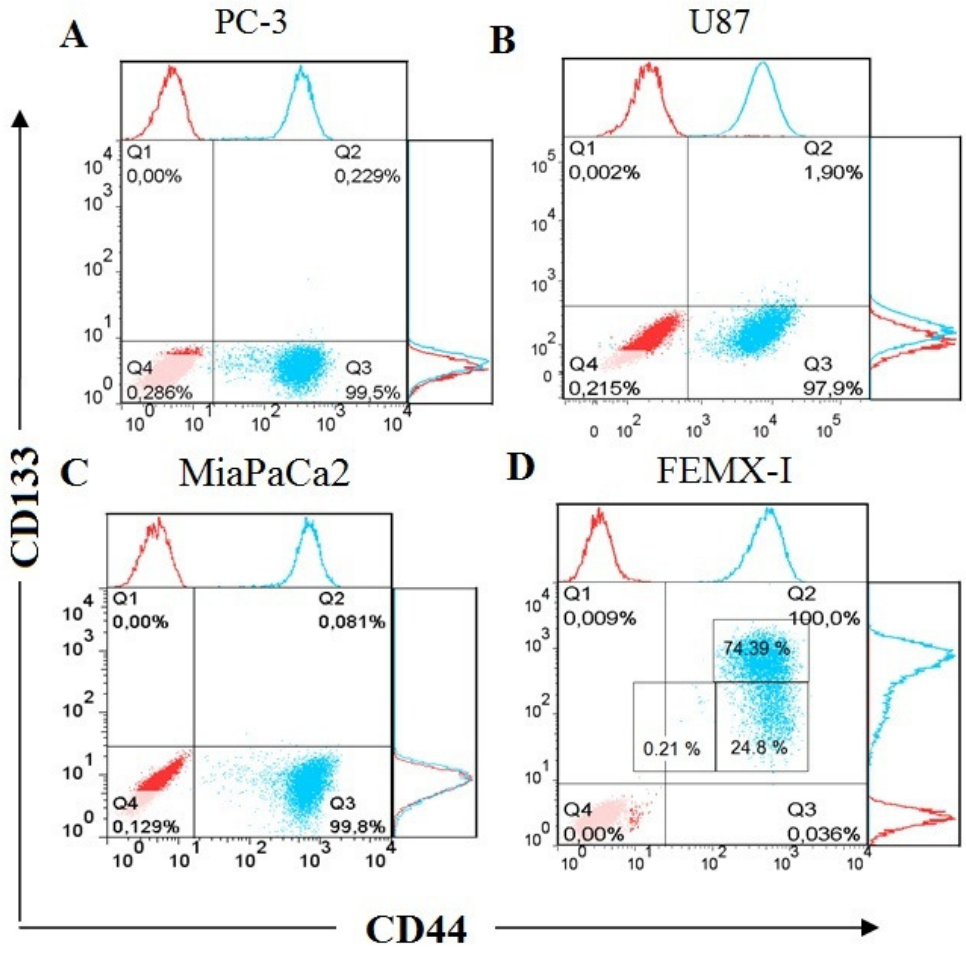

Fig. 3.1.1. The expression of CD133 and CD44 in different human cancer cell lines. Prostate adenocarcinoma (**A**), glioblastoma (**B**), pancreatic adenocarcinoma (**C**), and melanoma cells (**D**).

expression of CD133 was very low among these cell lines (0.001–0.23%) with slightly higher prevalence in U87 cells (1.94%, Fig. 3.1.1, B). Only FEMX-I cells exhibited high levels of CD133 (99.1%, Fig. 3.1.1, D).

The response to CD markers was not enough to determine heterogeneity of the cell lines. Therefore, we further analyzed the shape of their phenotypical patterns (Fig. 3.1.1). U87 (Fig. 3.1.1, B) cells show nearly uniform semi-horizontal oval-shaped cloud distribution. PC3 (Fig. 3.1.1, A) and MiaPaCa2 (Fig. 3.1.1, C) cells show two clouds, indicating two subpopulations: circular-shaped dense cloud with high CD44 expression ($CD44^{high}$) and a horizontal oval cloud with low/no CD44 expression ($CD44^{low/-}$). FEMX-I cells appear to consist of three different subpopulations: $CD44^{high}CD133^{high}$, $CD44^{high}CD133^{low/-}$, and $CD44^{low/-}CD133^{low/-}$ (Fig. 3.1.1, D).

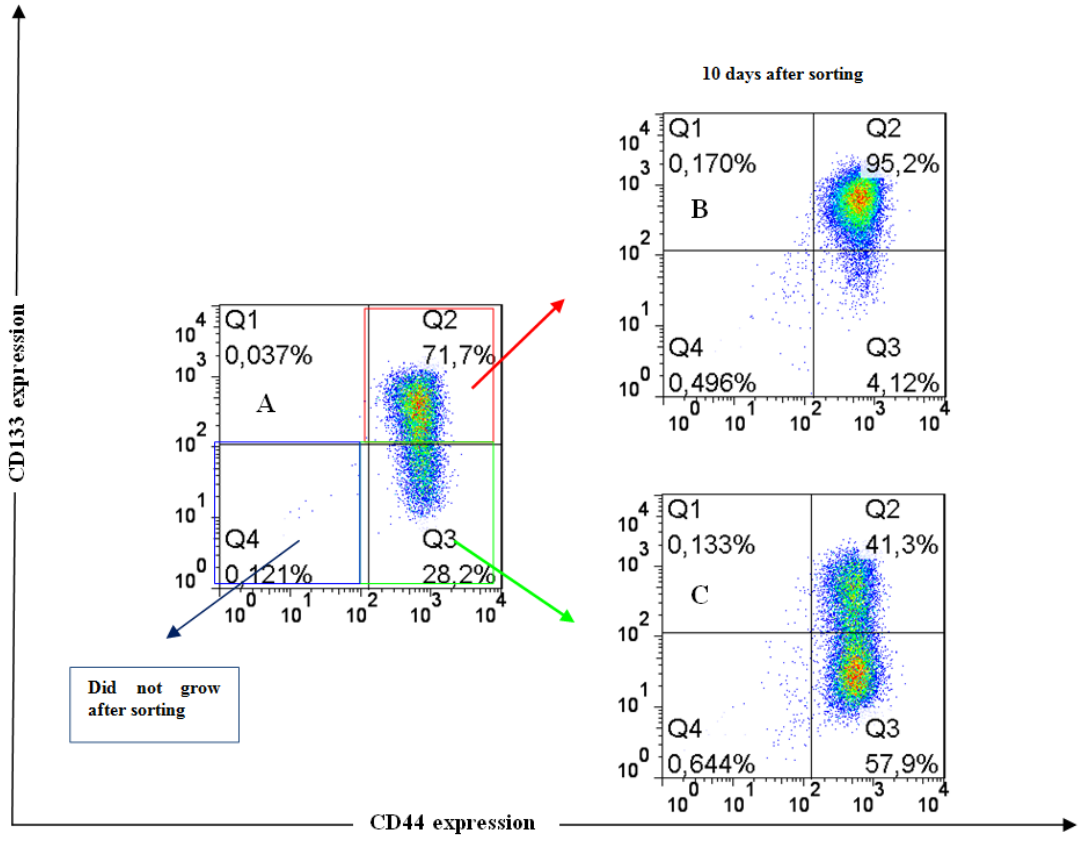

Fig. 3.1.2. The expression of CD133 and CD44 after FACS sorting of different subpopulations of FEMX-I cells. Phenotype of the total population of the cells before sorting (**A**), and phenotype of $CD44^{high}CD133^{high}$ (**B**), and $CD44^{high}CD133^{low/-}$ (**C**) subpopulations after 10 days growth after sorting.

Since FEMX-I cells showed high expression of both CD markers with three distinct subpopulations, we further examined their capability of growing and restoring initial population. Each subpopulation ($CD44^{high}CD133^{high}$, $CD44^{high}CD133^{low/-}$, and $CD44^{low/-}CD133^{low/-}$) was FACS sorted, isolated, and plated under usual growing conditions. $CD44^{low/-}CD133^{low/-}$ cells did not grow after sorting. $CD44^{high}CD133^{high}$ cells grew after sorting, but after 10 days of growth the cells did not show significant changes in their phenotypical composition. Immediately after sorting, the subpopulation was composed of ~95% $CD44^{high}CD133^{high}$ cells and remained unchanged after 10 days of growth (Fig. 3.1.2, A, B) suggesting that $CD44^{high}CD133^{high}$ subpopulation was unable to restore its progeny. However, $CD44^{high}CD133^{low/-}$ cells were able to grow and change their phenotypical composition. Immediately after sorting, the cells were composed of ~80% $CD44^{high}CD133^{low/-}$ cells, and after 10 days of growth this subpopulation was composed of ~58% $CD44^{high}CD133^{low/-}$ and ~41% $CD44^{high}CD133^{high}$ cells, thus approaching the phenotypical composition of the unsorted cells (Fig. 3.1.2, A, C).

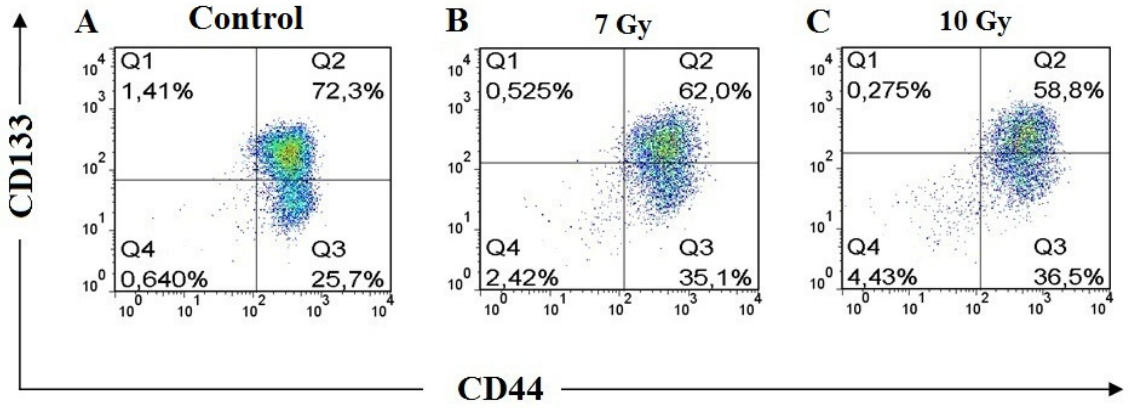

Fig. 3.1.3. The expression profiles of CD133 and CD44 shown separately for untreated cells (**A**) and for cells irradiated with 7 Gy (**B**) and 10 Gy (**C**). Different colors of the dots show the number of the overlapping dots: the red dots represent denser areas than the blue dots.

The doses (7 and 10 Gy) of ionizing radiation were chosen to induce death of more than half of the cells [28]. The percentage of the $CD44^{high}CD133^{high}$ subpopulation decreased from 72% in the control unirradiated cells to 58–62% after irradiation while

that of the subpopulation $CD44^{high}CD133^{low/-}$ increased from 26% to 35–36%. The percentage of $CD44^{low}CD133^{low/-}$ subpopulation increased from 0.6% in the untreated cells to ~2.4–4.4% in the cells after irradiation (Fig. 3.1.3, A-C).

To sum up, these results indicate that only $CD44^{high}CD133^{low/-}$cells are capable of progeny formation after sorting and are more resistant to radiotherapy treatment, therefore these cells posses more stem-like properties than $CD44^{high}CD133^{high}$ cells. Since CD133 are often reported to be the CSC-identifing marker [12, 29-31], our findings are controversal. But there are other studies which also find CD133 antigen as meaningless in detection of CSCs [15].

3.2. Accumulation of CdTe-MPA QDs in subpopulations of FEMX-I cells

To determine the accumulation of CdTe-MPA QDs in the subpopulations of FEMX-I cells, FEMX-I cells were incubated with QDs for 24 hours in the incubator (5% CO_2, 37º). Following incubation cells were brought into suspension and the immunophenotyping with anti-CD133-PE and anti-CD44-FITC markers were performed. Then the subpopulations of $CD44^{high}CD133^{low/-}$and $CD44^{high}CD133^{high}$ were gated out for the analysis of QDs emission inside them. The PL of QDs was registered in 94–99% of cells in both $CD44^{high}CD133^{low/-}$ and $CD44^{high}CD133^{high}$ subpopulations (Fig. 3.2.1).

These results indicate, that despite stem-like properties CdTe-MPA QDs accumulate inside cells. The accumulation of various types of QDs is well documented in many studies [19], however there is no information about the accumulation of QDs in CSCs. The reason for this might be the toxicity of CdTe-MPA, which is shown in many publications [28, 32-34]. But it is important to mention that toxicity is associated with the release of the ions of Cd and Te. Recently this instability issue had been solved by capping the core of QDs with additional coatings [35-37]. By using well coated QDs, scientists demonstrated successful labeling of normal stem cells, without any disturbance into its physiological functions [38, 39].

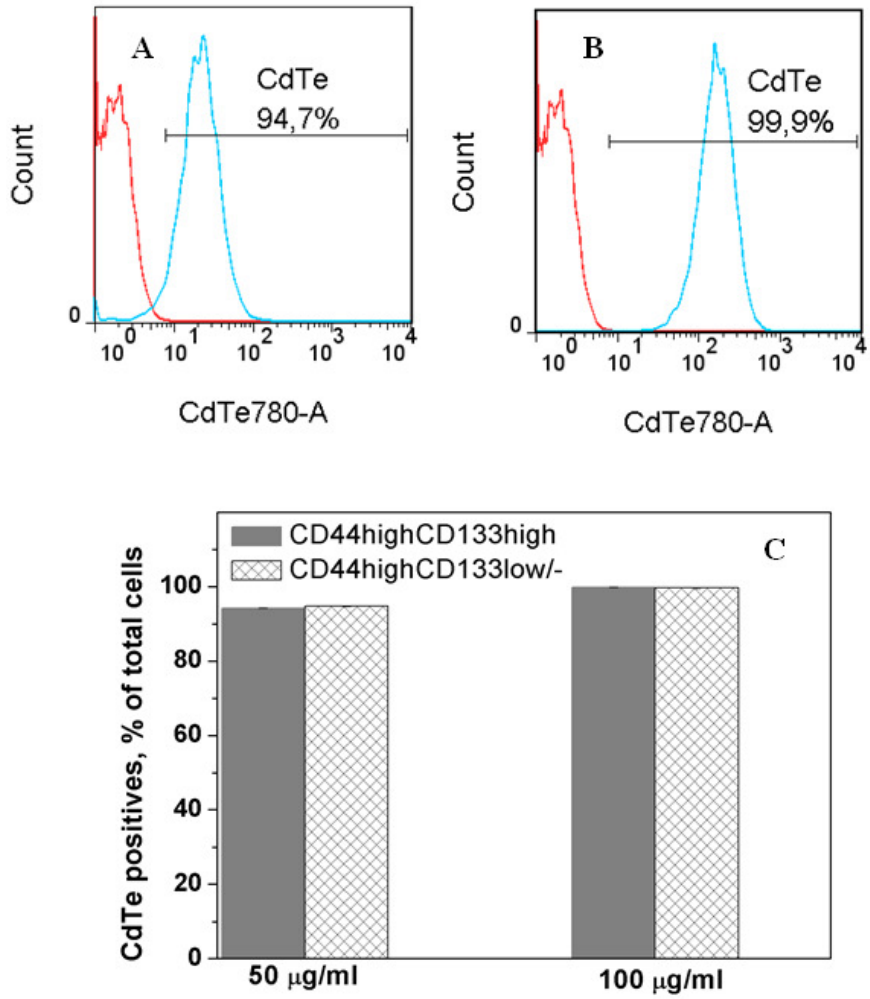

Fig. 3.2.1. Accumulation of the CdTe-MPA QDs in FEMX-I cells. Intensity histograms represent autofluorescence of the control untreated cells (red curve) and the fluorescence of the cells treated with 50 μg/ml (**A, blue curve**) and 100 μg/ml (**B, blue curve**) QDs, respectively. The percentage of cells positive for QDs PL was 94–99% in all subpopulations (**C**).

3.3. Accumulation of non-functionalized QDs and anti-CD44-QD conjugates in breast cancer cells

Accumulation of non-functionalized carboxyl-coated QDs studies showed that MCF-7 and MDA-MB-231 breast cancer cells accumulate QDs and store them in endocytic vesicles (Fig. 3.3.1). Confocal fluorescence images taken at 3, 6 and 24 hours

after the incubation with carboxyl-functionalized QDs at 37˚C show that the localization and distribution of vesicles with QDs depends on the incubation time: after 3 hours vesicles are distributed all along the cell in MDA-MB-231 cells (Fig. 3.3.1, A), after 6 hours vesicles of QDs localize in the close proximity to the nucleus (Fig. 3.3.1, B) and after 24h multivesicular body-like structures with QDs are formed in the perinuclear region (Fig. 3.3.1, C). A slightly different time-dependent distribution is present in MCF-7 cells: after 3 hours vesicles with QDs are spread all over the cytoplasm and in the course of time their distribution almost does not change (Fig. 3.3.1, D-F). However, the size of the vesicles differs between cell lines – MDA-MB-231 cells form over 2 times larger vesicles than MCF-7 cells.

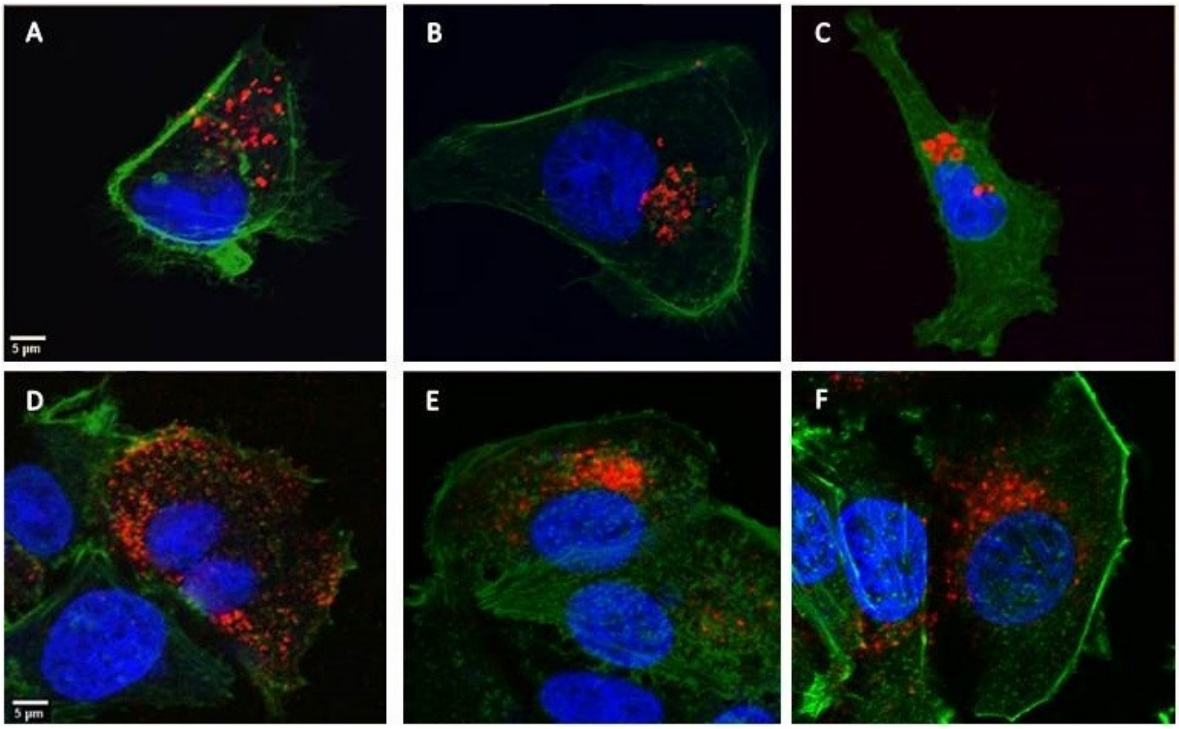

Fig. 3.3.1. MDA-MB-231 cells (top) and MCF-7 cells (bottom) after 3h, 6h and 24h incubation with non-functionalized QDs. Green color shows **actin**, blue color – **nucleus**, red color – **QDs**.

Accumulation of QDs in different types of cells have been well documented. Similary to our results, other authors find QDs to localize in endocytic vesicles with slight differences between various types of cell [40]. However, the information about accumulation and localization of antibody-functionalized QDs is still missing. Therefore

we futher performed accumulation and distribution studies of anti-CD44-QDs in both $CD44^+$ (MDA-MB-231) and $CD44^-$ (MCF-7) cancer cells.

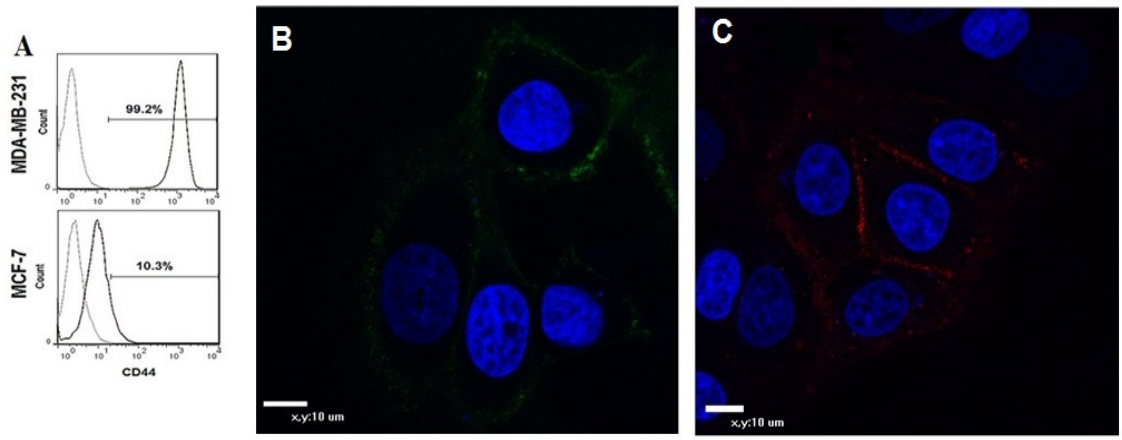

Fig. 3.3.2. The expression of CD44 surface antigen of MDA-MB-231 and MCF-7 cells (**A**). Laser scanning confocal micrographs of MCF-7 cells after 30 min incubation with anti-CD44-QD (**C**) and anti-CD44-FITC (**B**). Blue color shows **nucleus**, green color – **anti-CD44-FITC**, red color – **anti-CD44-QD.**

As seen from flow cytometry results, MCF-7 cells express CD44 molecule weakly – only 10,3% of MCF-7 cells express CD44 adhesion molecule and has fewer CD44 antigens than MDA-MB-231 cells (Fig. 3.3.2A). After incubation with anti-CD44-QDs and anti-CD44-FITC, only a weak PL signal is registered in the plasma membrane of MCF-7 cells (Fig. 3.3.2B, C). That shows the specificity of used antibodies for binding CD44 antigens. Contrary, strong labelling is registered in the MDA-MB-231 ($CD44^+$) cells: after 30 min incubation the anti-CD44-QDs and anti-CD44-FITC brightly and continuously label plasma membrane of the cells (Fig. 3.3.3, left panel). Interestingly, after 24 hours post labeling, redistribution is registered in the anti-CD44-QD-labeled cells: while antibodies conjugated with FITC stay in the cell membrane, the anti-CD44-QDs conjugates are engulfed and packed into vesicles (Fig. 3.3.3, right panel), similarly as in the case of non-targeted QDs (Fig. 3.3.1).

In conclusion, the accumulation results of anti-CD44-QDs in $CD44^+$ and $CD44^-$ cells show the selectivity of targeted nanoparticles. Moreover, the engulfment of anti-CD44-QDs inside cells shows the capability of QDs not only to selectively label CSC-

like cells, which is very important for NP applications in cancer imaging, but also it shows the capacity of QDs as a drug transporter. It is unknown, why QD-conjugated antibody is engulfed inside cells, while organic molecule FITC-conjugated antibody

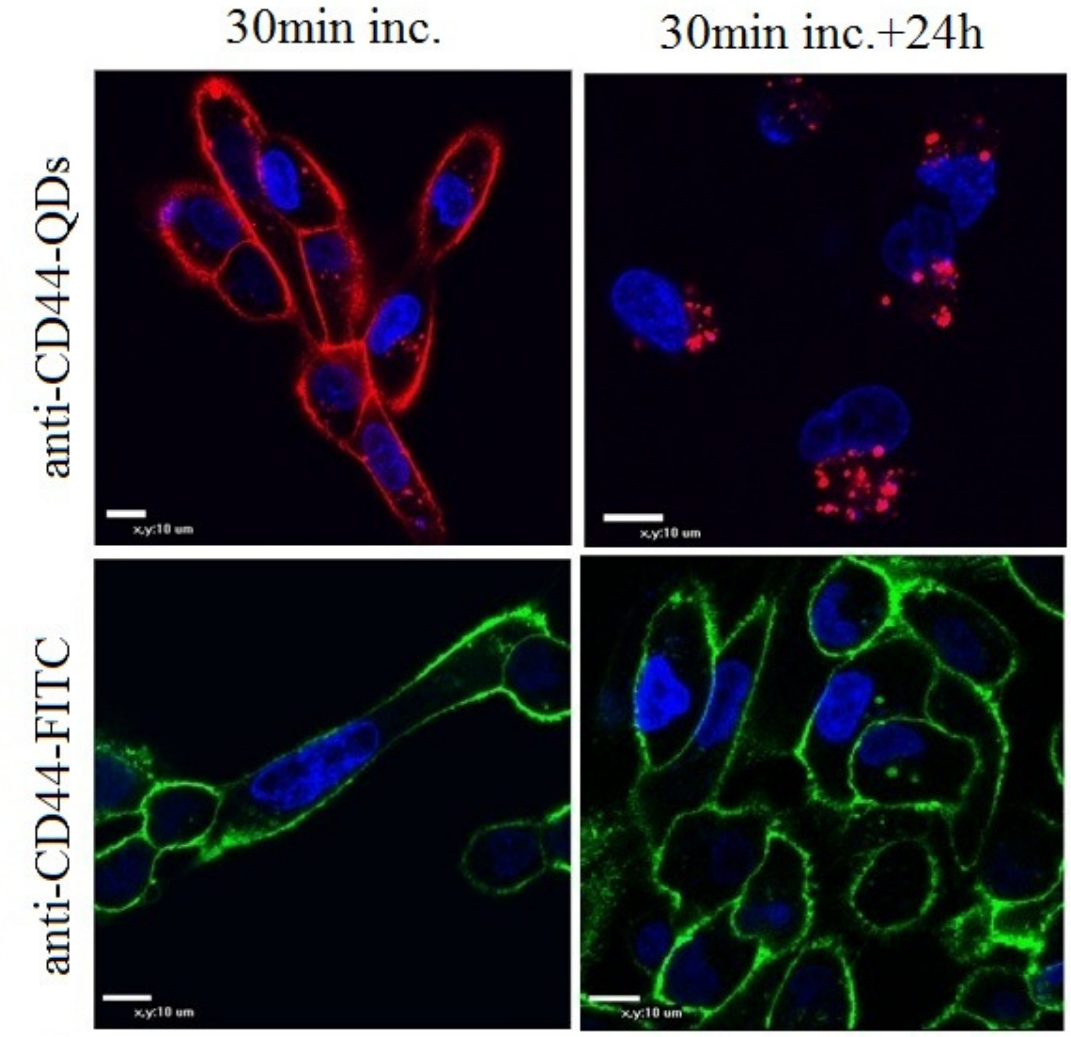

Fig. 3.3.3. Laser scanning confocal micrographs of the stem-like MDA-MB-231 cells after 30 min incubation with **anti-CD44-QDs** (red) and **anti-CD44-FITC** (green) and after additional cultivation post incubation under standart culture conditions for 24h. Blue color shows **nucleus**.

remains in plasma membrane. The size of QD might be a reason as it resembles the size of CD44 ligand – hyaluronic acid, but futher studies are needed to give a reasonable explanation. Other studies with QD-bioactive molecule conjugates revealed that conjugates accumulate more efficiently in cancer cells, then unconjugated QDs [21, 22,

41]. However, no studies concerning distribution of QD-conjugates *in vitro* or *in vivo* have been found. Therefore our study gives new knowledge in the field of nanomedicine.

3.4. Cellular uptake and photosensitizing properties of quantum dot-chlorin e_6 complex in MiaPaCa2 cancer cells

Schematic representation of QD-Ce_6 complex formation can be seen in Fig. 3.4.1A. The size and location of Ce_6 molecules as well as the size of QDs and its inner core/shell (6.1±0.4 nm) are drawn to scale according to Jennings *et al* and our previous findings [42, 43]. The formation of the QD-Ce_6 complex in aqueous solution was determined spectroscopically. The addition of Ce_6 into the aqueous solution of QDs induced the decrease in intensity of a PL band of QDs with simultaneous appearance of the Ce_6 fluorescence band in the complex with a maximum at 670 nm, which is bathochromically shifted in comparison with the fluorescence maximum at 660 nm of free Ce_6 (Fig. 3.4.1, B). The broad absorption spectrum of the QDs [44] enabled us to find a suitable wavelength for the energy transfer studies where the donor QDs could be selectively excited avoiding the direct excitation of Ce_6. Thus, the detected increase of fluorescence intensity of Ce_6 at 670 nm with accompanying decrease of the PL intensity of QDs at 607 nm indicate the excitation energy transfer from QDs to Ce_6 molecules in the complex.

Steady state spectroscopy observations have been supported by the PL lifetime measurements. The mean PL lifetime $<\tau>$ of pure QDs was found to be 26.3 ns and decreased to 16.7 ns in the presence of Ce_6 at a molar ratio1:5 (Fig. 3.4.1, C). A substantial shortening of the donor QDs lifetime in the presence of the acceptor Ce_6 accords with the quenching of QDs PL intensity by Ce_6 in the formed complex implying the FRET mechanism.

For the accumulation studies QD-Ce_6 complex was prepared as previously described and poured over the cells. For comparison, pure QDs and pure Ce_6 were applied on the cells separately at the same concentrations. Images were recorded by laser scanning confocal microscopy with the upgrade of spectral imaging and fluorescence lifetime imaging units.

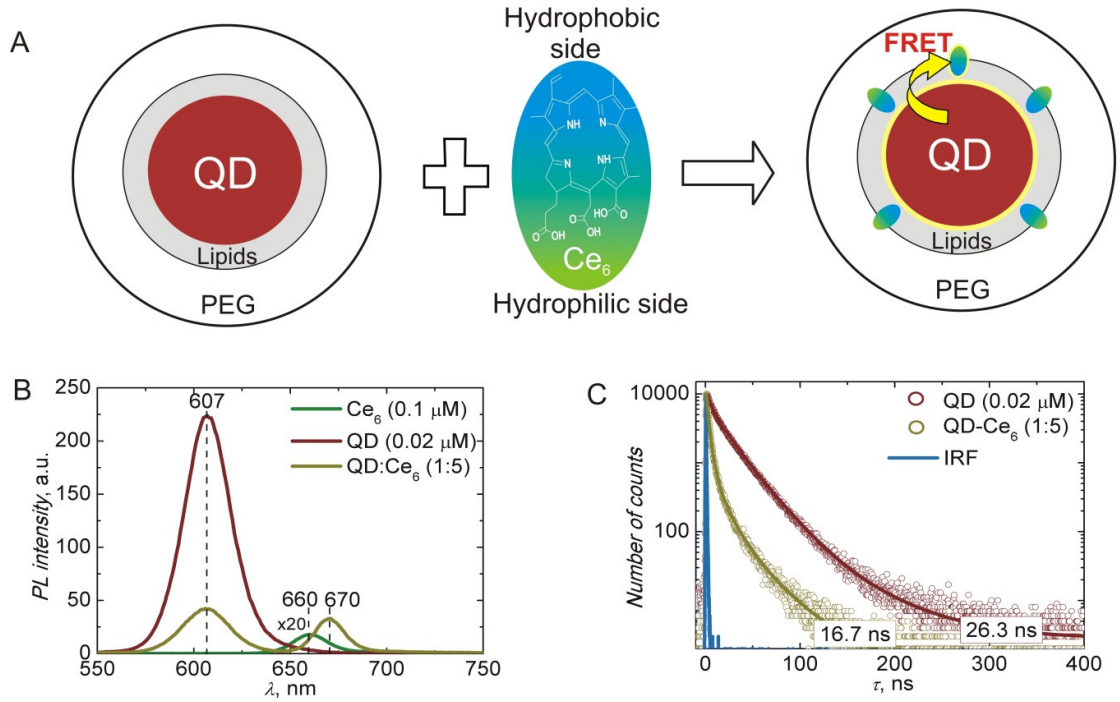

Fig. 3.4.1. Schematic representation of QD-Ce_6 complex formation (**A**), where the size and location of Ce_6 molecules as well as the size of QDs and its inner core/shell are drawn to scale. PL spectra (**B**) of pure QDs, Ce_6 and QD-Ce_6 solution at QD:Ce_6 molar ratio 1:5. PL spectrum of pure Ce_6 is multiplied 20 times; PL decay spectra (**C**) (λ_{ex} = 405 nm, λ_{em} = 605 nm) of pure QDs and QD-Ce_6 solution. Instrument response function (IRF) is also shown.

Ce_6 molecules distribute diffusely in the cells (Fig.3.4.2, A). The spectral analysis revealed that the fluorescence band of Ce_6 in live cells is shifted to the red (λ_{max}=670 nm) (Fig.3.4.2, A, insert) in comparison to aqueous solution (λ_{max}=660nm) (Fig.3.4.1, A). Due to amphiphilic structure of Ce_6 molecule, its spectral properties are highly sensitive to environmental changes. Upon interaction with hydrophobic compartments of cell membranes and inner proteins, the PL spectrum of Ce_6 experiences a bathochromic shift [45, 46]. Distribution of QDs in cells has a more discrete pattern (Fig. 3.4.2, B). QDs localize in the plasma membrane and vesicles.

Accumulation of QD-Ce_6 complex in cells is presented in Fig. 3.4.2 C. Green-, yellow- and red-coloured regions are detected inside cells. For more precise analysis, the spectral data were extracted for yellow (1), green (2) and red (3) regions (Fig. 3.4.2, D). Interestingly, the PL of QD-Ce_6 complex was in detected all coloured regions, but with

different QD:Ce_6 PL intensity ratios (Fig. 3.4.2, D). Yellow regions represent areas where QD:Ce_6 PL intensity ratio is similar to that registered in aqueous solution (Fig. 3.4.1, B**).** Green regions are seen in plasma membrane and few vesicles and represent the

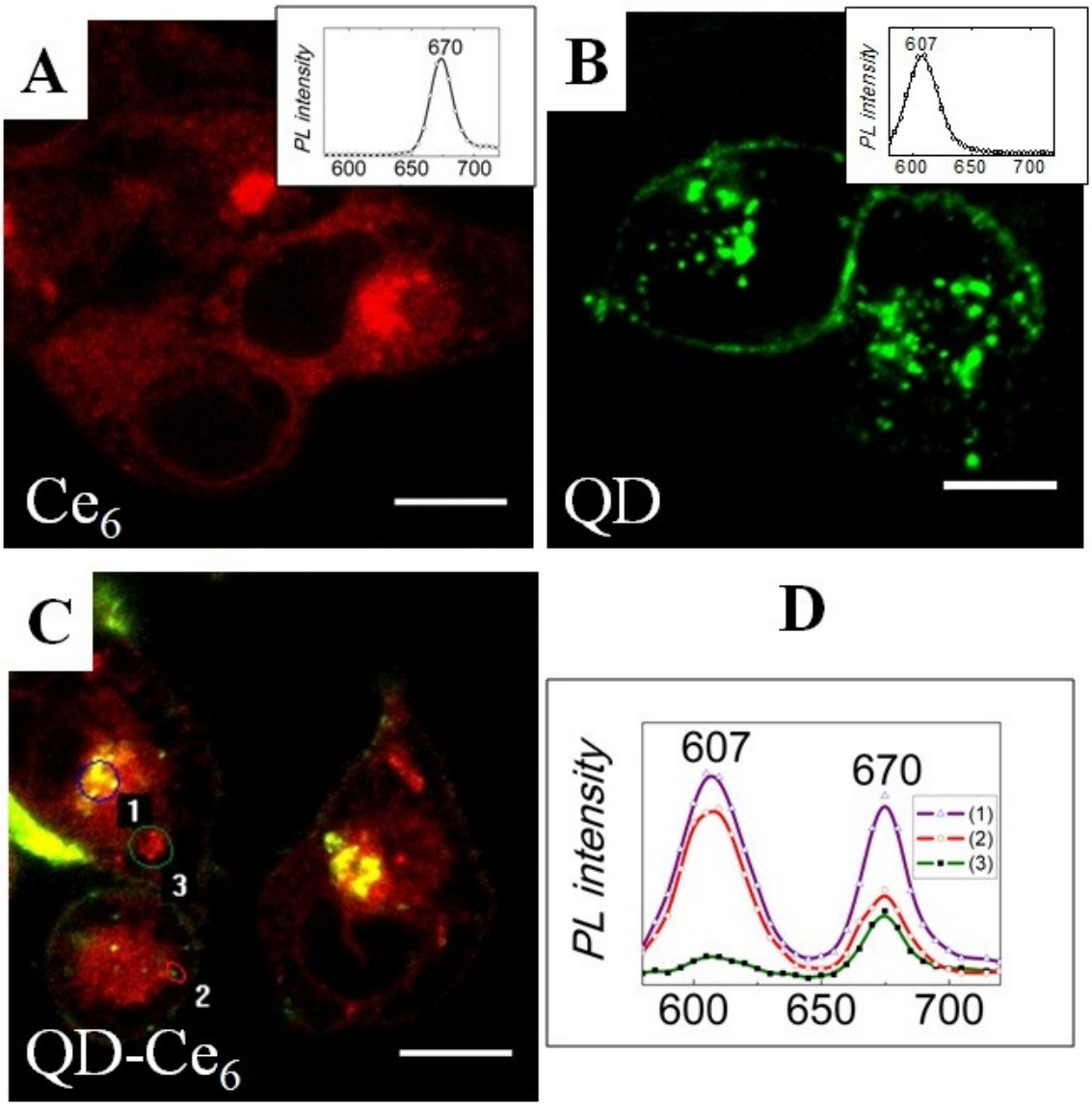

Fig. 3.4.2. Intracellular distribution of Ce_6 (A), QDs (B) and QD-Ce_6 complex (C) in MiaPaCa2 cells under spectral confocal microscope (λ_{ex} = 488 nm). Scale bar = 10 µm. Red color shows **Ce_6**, green color – **QDs**, yellow color shows **colocalization** of red and green emission.

higher PL intensity of QDs (at λ=607 nm) in the QD-Ce_6 complex. It is known that quenching of QDs PL in the QD-Ce_6 complex depends on the number of bound Ce_6

molecules [47], therefore green regions indicate areas where QD-Ce_6 complex underwent partial loss of Ce_6 molecules during intracellular uptake. Red regions are seen in vesicles and diffusely spread through the cell representing the superposition of the QD-Ce_6 PL as well as the fluorescence of Ce_6 possibly released from the complex due to the interaction with the cell substrate.

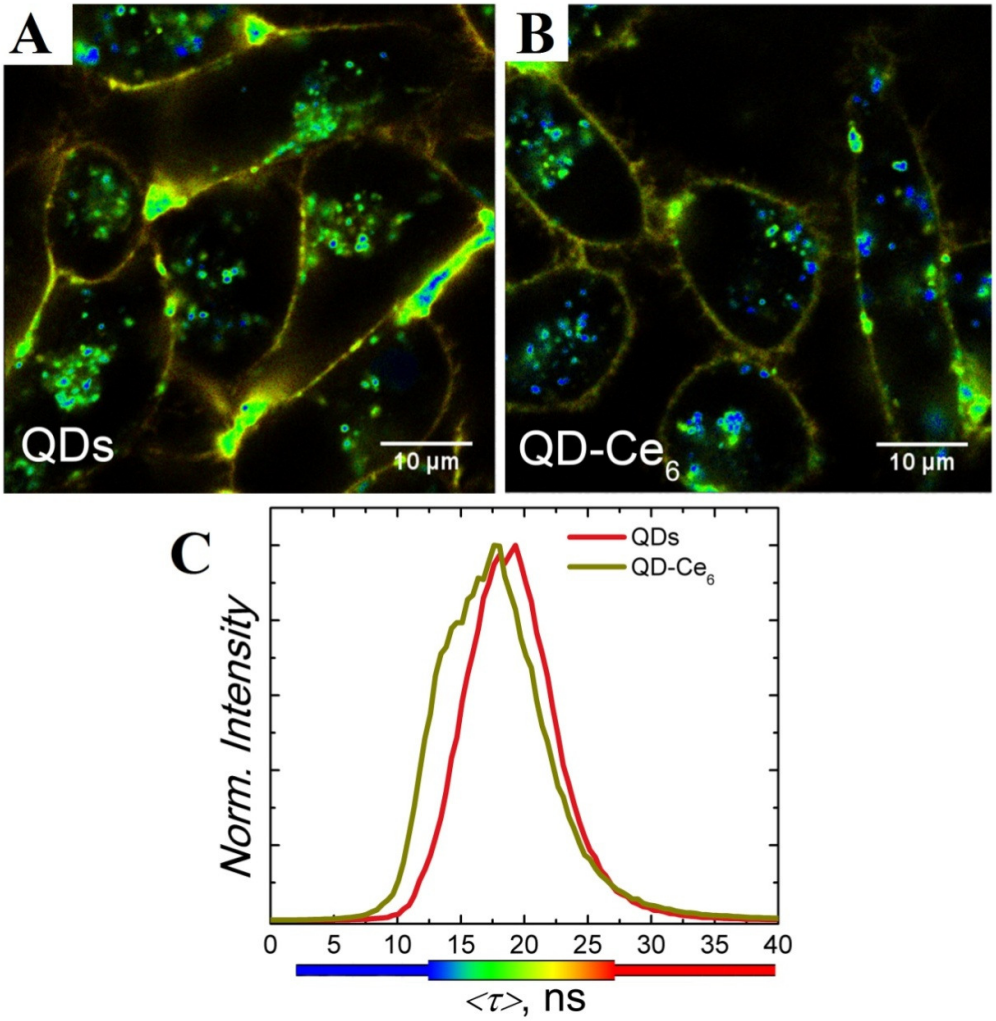

Fig. 3.4.3. FLIM of QDs and QD-Ce_6 complex (**A**) in MiaPaCa2 cells (λ_{ex} = 404 nm). (**B**) - plotted histograms for obtained average lifetimes of QDs (red curve) and QD-Ce_6 complex (yellow curve). Colours of FLIM images in A and B correspond to lifetime values presented in (**C**) (colour scale).

The shortening of the mean PL lifetime <τ> was also found during FLIM measurements of cells incubated with QD-Ce_6 complex, as represented in Fig. 3.4.3,

where the bluish and greenish colours have been attributed to the areas with shorter and longer <τ>, respectively. The lifetime image of QDs yielded few colours in one cell indicating longer PL lifetimes in plasma membrane and shorter PL lifetimes inside inner organelles. After incubation with QD-Ce_6 complex more vesicles with shorter PL lifetimes appeared (Fig.3.4.3 B, blue colour), reflecting quenching due to energy transfer from QDs to Ce_6 molecules, and at the same time verifying the presence of QD-Ce_6 complex inside cancer cells.The quantitative analysis was done by calculating PL lifetime histograms for each image. The mean PL lifetime <τ> of QDs in cells was found to be 19 ns and decreased to 16 ns in the cells incubated with QD-Ce_6 complex.

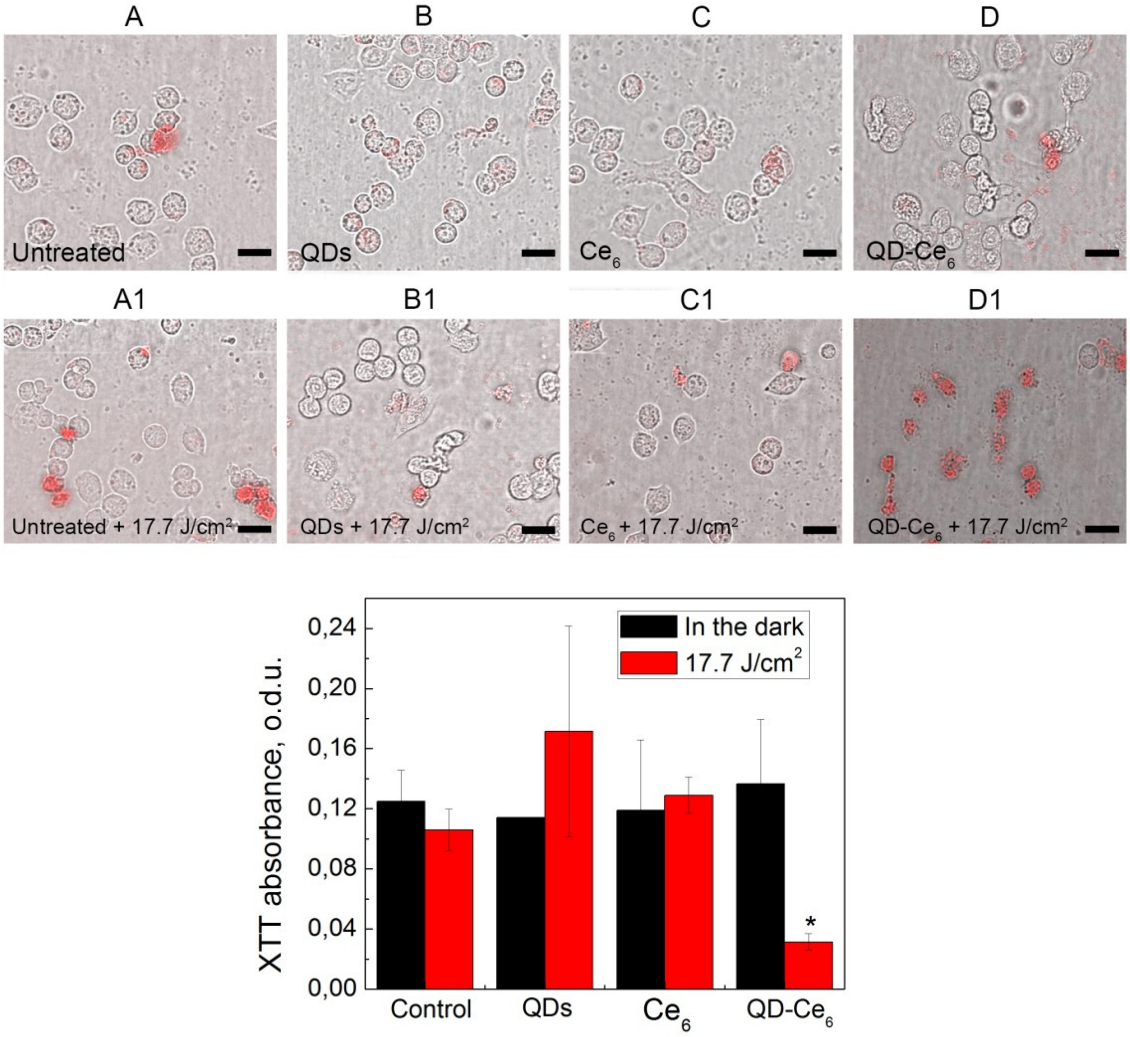

Fig. 3.4.4. MiaPaCa2 cells after treatment with QDs, Ce_6 and QD-Ce_6 complex in the dark (**A, B, C, D**) and after 17.7 J/cm^2 irradiation (470 nm) respectively (**A1, B1, C1, D1**). After combined treatment (complex+irradiation), all cells were stained with

propidium iodide (red). Scale bar – 10 μm. Histogram shows XXT absorbance after treatmentwith QDs, Ce_6 and QD-Ce_6 complex in the dark and in the precence of 17.7 J/cm^2 irradiation. *P<0.05.

As it was shown in accumulation studies, QD-Ce_6 complex localize in plasma membrane and vesicles within three hours. To determine whether such subcellular localization of the complex is proper to induce cell death via FRET, the cells were exposed to 17.7 J/cm^2 irradiation at 470 nm, where the absorbance of QDs is dominant [44]. As can be seen in Fig. 3.4.4, the viability of MiaPaCa2 changed dramatically only in those cells, which was incubated with QD-Ce_6 complex and irradiated by light dominantly absorbed by the QDs. The microscopy image (Fig. 3.4.4, D1) shows randomly shaped, propidium iodide stained cells. Such observations are not present in irradiation untreated cells (Fig. 3.4.4, A, B, C, D) as well as all other controls (Fig. 3.4.4 A1, B1, C1) and are indicative of obvious cell mortality. Quantitative analysis correlated with microscopy results: the combined treatment of cells with QD-Ce_6 complex and irradiation resulted in ~4 times lower viability and proliferation (Fig. 3.4.4).

Since nanotechnologies immerged into medicine as a potential therapeutic upgrade to conventional therapies, the development of newer photoactive agents in PDT using nanoparticles have become of great interest [48-51]. Combination of semiconductor nanocrystals, namely QDs, and PS might resolve many difficulties that are encountered in PDT, such as specific localization in cancerous tissue, excitation of PDT agents via energy transfer and visualization of therapy. We have preliminary data that shows QD-PS complex accumulation in cells within 3 hours. The complex localize into vesicles of cancer cells without losing the ability to transfer energy from QDs to chlorin e_6 via FRET. Nevertheless, after QD-selective irradiation at 470 nm QD-Ce_6 complex showed phototoxicity in MiaPaCa2 cancer cells without significant dark toxicities.

4. CONCLUSIONS

1) Analysis by flow cytometry revealed, that $CD44^{high}CD133^{low/-}$ subpopulation of melanoma cells FEMX-I is capable of restoring its initial unsorted composition as well as is less sensitive to ionizing radiation, therefore $CD44^{high}CD133^{low/-}$ cells can be used as a model system of CSCs in the development of anti-cancer agents.

2) Although cancer cells are different in terms of chemo- and radiosensitivity, expression of surface proteins, capability to form colonies *in vitro* and tumors *in vivo*, they uptake quantum dots in a similar manner: quantum dots are engulfed in a concentration-dependent way and packed into vesicles in the perinuclear region.

3) Due to higher PL intensity and non-toxic behaviour, CdSe/ZnS-(AMP)-COOH QDs are more suitable for application of nanocomposites in the imaging of cancer stem cells.

4) Conjugates of CdSe/ZnS-(AML/PEG)-COOH QDs and anti-CD44 are packed into vesicles selectively inside $CD44^+$ cells, while anti-CD44-FITC conjugates remain on the plasma membrane. Engulfement of anti-CD44-QDs might show its capability to bring „cargo“ inside the selected type of cells.

5) Analysis by laser scanning spectral confocal and fluorescence lifetime imaging microscopy revealed, that the complex of CdSe/ZnS-(AML/PEG)-COOH QDs and photosensitizer chlorin e_6 accumulates inside plasma membrane and vesicles of cancer cells. Such a subcellular localization is proper enough to initiate light-mediated cell death via energy transfer from QDs to Ce_6 molecules. These results show the capability of QDs to act not only as a fluorescent label but also as a therapeutic agent.

6) When incubation of the non-covalent CdSe/ZnS-(AML/PEG)-COOH-Ce_6 complex is conducted in culture medium vs physiological saline, better stability and energy transfer is registered inside cells.

5. SANTRAUKA

Įvadas

Nepaisant pažangos vėžio gydymo srityje, daugelis mokslininkų ir tyrėjų pripažįsta, kad šiuo metu taikomos standartinės terapijos pasižymi žemu gydymo efektyvumu,o vėžio atsinaujinimas po taikytos terapijos išlieka opi gydymo problema. Pasaulinio vėžio registro duomenimis, sergančiųjų šia klastinga liga vis daugėja: 2012 metais užregistruota ~14 milijonų sergančiųjų vėžiu ir progozuojama, jog šis skaičius 2035 metais sieks 24 milijonus. Atliktų fundamentaliųjų darbų bei mokslo tyrimų rezultatai rodo, kad už prastą gydomąjį efektą, metastazes bei naviko atsinaujinimą po taikyto gydymo gali būti atsakinga vėžinių ląstelių subpopuliacija, pasižyminti kamieninių ląstelių savybėmis. Šios subpopuliacijos vėžinės ląstelės pasižymi genų raiškos pokyčiais ir/ar mutacijomis, susijusiomis su apoptozės slopinimu, proliferacijos aktyvinimu, molekulių transportavimo ir vaistų šalinimo iš ląstelės mechanizmų įjungimu. Todėl daroma prielaida, kad nuo vėžinių kamieninių ląstelių, pasižyminčių aktyviais molekuliniais rezistentiškumo mechanizmais, priklauso atsparumas taikomai terapijai bei metastazių formavimasis. Ekspertų, dirbančių onkologijos srityje, nuomone, efektyvios vėžio terapijos taikinys turėtų būti vėžinės kamieninės ląstelės (VKL). VKL aptikimas ir toksinio poveikio joms realizavimas leistų padidinti onkologinių susirgimų gydymo veiksmingumą ir specifiškumą bei padėtų išvengti antrinių navikų ir metastazių.

Spartus nanomedicinos vystymąsis jau šiandien pateikia įvairius onkologinių problemų sprendimo kelius. Nanodalelės ar nanodariniai pasižymintys išskirtinėmis savybėmis sėkmingai taikomi eksperimentinėje klinikoje, tad neabejotinai aktualus ir nanodarinių sąveikos su VKL klausimas sprendžiant neinvazinės diagnostikos ir tikslinio vaisto nuvedimo į pažaidos vietą įgyvendinimą. Jau dabar aptinkama straipsnių, kuriuose parodoma, kaip sėkmingai yra įveikiamos chemoterapijai ir radioterapijai atsparios VKL nanotechnologijų pagalba. Todėl VKL aptikimas, nanotechnologijų sintezė, modifikavimas ir tyrimai įvairaus tipo vėžinėse ląstelėse yra svarbūs šių dienų moksliniai uždaviniai.

Tyrimo tikslas

Ištirti nanodarinių pritaikymo galimybes vėžinių kamieninių ląstelių aptikimui ir sunaikinimui.

Uždaviniai:

1) Ištirti CdTe-MPA kaupimąsi melanomos kamieninėse ląstelėse;
2) Palyginti CdTe-MPA ir CdSe/ZnS-(AMP)-COOH kaupimąsi ir poveikį žmogaus vėžinių ląstelių linijose;
3) Ištirti CdSe/ZnS-(AML/PEG)-COOH ir antikūno prieš CD44 antigeną konjugato kaupimosi ir pasiskirstymo dėsningumus krūties vėžinėse kamieninėse ląstelėse.
4) Ištirti CdSe/ZnS-(AML/PEG)-COOH ir sensibilizatoriaus Ce_6 komplekso kaupimąsi, energijos pernašą ir sensibilizacinį poveikį *in vitro*;
5) Įvertinti CdSe/ZnS-(AML/PEG)-COOH ir sensibilizatoriaus Ce_6 komplekso stabilumą baltymais prisotintoje mitybinėje terpėje, imituojant *in vivo* sistemos kraujotaką;

Ginamieji teiginiai:

1) Melanomos ląstelių linijos FEMX-I $CD44^{daug}CD133^{mažai/-}$ fenotipo subpopuliacija pasižymi vėžinėms kamieninėms ląstelėms būdingomis savybėmis.

2) Nepaisant skirtingų kamieniškumo savybių, KT kaupimosi dėsningumai beveik vienodi visose vėžinėse ląstelėse: KT patenka į ląstelių citoplazmą, išsidėsto ląstelėje pūslelinėmis struktūromis aplink branduolį, o didinant KT koncentraciją, matomas didesnis KT fotoliuminescencijos intensyvumas ląstelėse.

3) CdSe/ZnS-(AMP)-COOH KT pasižymi didesniu fotoliuminescencijos intensyvumu ląstelėse ir mažesniu toksiniu poveikiu joms nei ZnS sluoksnio ir AMP dangalo neturintys CdTe-MPA KT.

4) Antikūnais prieš paviršiaus antigeną CD44 padengti CdSe/ZnS-(AML/PEG)-COOH KT selektyviai patenka į $CD44^+$ fenotipo, kuris būdingas krūties vėžinėms kamieninėms ląstelėms, vidų ir pasiskirsto pūslelėse aplink branduolį, o anti-CD44, konjuguotas su organine fluorescuojančia molekule, nepatenka į ląstelių vidų ir bėgant laikui lieka prisijungęs prie ląstelės plazminės membranos.

5) Sensibilizatoriaus chlorino e_6 ir CdSe/ZnS-(AML/PEG)-COOH KT kompleksas per 3 valandas susikaupia plazminėje membranoje ir vėžinių ląstelių viduje, pūslelinėse struktūrose, o paveikus regimąja šviesa geba sukelti vėžinių ląstelių žūtį per energijos pernašą iš KT į chloriną e_6.

6) Nekovalentiškai sujungtas CdSe/ZnS-(AML/PEG)-COOH KT ir Ce_6 nanodarinys yra stabilesnis ląstelėse, kai inkubacija atliekama baltymais ir vitaminais prisotintoje, *in vivo* sistemą primenančioje terpėje, nei fiziologiniame druskų tirpale.

Aktualumas ir naujumas

Tiek pasaulyje, tiek Lietuvoje onkologinių susirgimų vis daugėja, o mirtingumas nuo vėžinių susirgimų yra antroje vietoje, po širdies ir kraujagyslių ligų. Tai verčia įvairių sričių mokslininkus apjungti savo žinias ir ieškoti ne tik ankstyvą vėžio diagnostiką užtikrinančių priemonių, bet ir išsiaiškinti priežastis bei mechanizmus, lemiančius vėžio atsparumą gydymui.

Pastarąjį 10-metį vis gausėja įrodymų apie vėžyje esančią nedidelę subpopuliaciją, pavadintą – vėžio kamieninėmis ląstelėmis. Teigiama, jog būtent VKL yra atsakingos už naviko formavimą, atsparumą taikomai terapijai bei metastazių formavimą [9-11]. Intensyviai ieškoma žymenų, kurie leistų aptikti „pavojingąsias“ ląsteles, bei sunaikinti jas, tokiu būdu užkertant kelią vėlesniam ligos atsinaujinimui ir progresavimui. Šiai dienai jau yra pasiūlyta nemažai žymenų, kurie galėtų aptikti VKL ląsteles įvairių lokalizacijų navikuose [12-14]. Tačiau vis dar yra ginčijamasi dėl žymenų patikimumo ir jų gebėjimo pažymėti visas VKL [15], dėl to norint atskirti/išgryninti „piktąsias“ ląsteles, atliekami kiti tyrimai, kurie parodo žymenimis atskirtų VKL gebėjimą formuoti navikus, gebėjimą migruoti, metastazuoti ir atsparumą chemoterapiniams vaistams bei jonizuojančiai spinduliuotei.

Nanodalelės pateikia naujas galimybes vėžio diagnostikos ir gydymo srityje. Ypač svarbi ND savybė – diagnostikos ir terapijos funkcijų apjungimas į vieną darinį. Diagnostiką ir terapiją atliekantys nanodariniai yra vadinami nauju terminu – teranostiniais nanodariniais [16]. Kvantiniai taškai mokslinėje literatūroje minimi kaip ryškiausiai šviečiantys fluorochromai, pasižymintys reguliuojamomis spektrinėmis savybėmis, leidžiančiomis pasirinkti sugerties ir emisijos spektrinius ruožus audinių

skaidrumo lange [17, 18]. Jų lengvai modifikuojamas paviršius leidžia užkabinti norimas bioaktyvias molekules, pavyzdžiui antikūnus, bei terapinę funkciją atliekančius vaistus – chemopreparatus ir fotosensibilizatorius [19, 20]. KT dengti peptidais ir antikūnais prieš EGFR antigeną, buvo sėkmingai panaudoti selektyviam vėžio aptikimui *in vivo* [21, 22]. Tačiau nepavyko rasti duomenų apie VKL žymenimis dengtų KT panaudojimą VKL aptikimui *in vitro* ir *in vivo*.

KT panaudojimas kaip diagnostiką ir terapiją atliekančio nanodarinio buvo pasiūlytas dar 2003 metais, kai Samia pristatė KT (kaip galimo šviesos energijos donoro) ir fotosensbilizatoriaus (šviesos akceptoriaus) apjungimą į kompleksą [23]. Tokia sistema leistų parinkti žadinančiąją spinduliuotę audinių skaidrumo lange, o prikabintas sensibilizatorius atliktų aktyvių deguonies formų generavimą, sukeldamas navikinių ląstelių žūtį. KT-FS nanodariniai buvo pasiūlyti ir kitų mokslininkų, buvo parodytas jų susikompleksavimas, gebėjimas perduoti energiją iš KT į FS, bei singuletinio deguonies generavimas [24, 25]. Tačiau vis dar trūksta duomenų apie KT-FS suderinamumą su biologine aplinka, jų kaupimąsi ir gebėjimą inicijuotį vėžinių ląstelių žūtį.

Šiame darbe pirmą kartą įvertintas FEMX-I ląstelių jautrumas jonizuojančiai spinduliuotei, įvertinta, jog KT kaupiasi neatsižvelgiant į imunofenotipinius ar funkcinius ląstelių skirtumus. Taip pat parodyta, jog antikūnais (prieš antigeną CD44, kuris būdingas VKL) dengti KT kaupiasi selektyviai tik $CD44^+$ ląstelėse, bei patenka į jų vidų, priešingai nei FITC dažu žymėtas analogiškas antikūnas. Pirmą kartą parodytas sukonstruoto KT ir sensibilizatoriaus chlorino e_6 komplekso kaupimasis, energijos pernaša ir inicijuota ląstelių žūtis vėžinėse ląstelėse. Šie rezultatai parodo KT galimybes tiek selektyviai diagnostikai, tiek terapijai. Ateityje bus siekiama apjungti abi funkcijas (selektyvaus kaupimosi ir terapijos) į vieną KT nanodarinį ir taip priartėti prie norimo nanotechnologinio teranostinio preparato.

Pagrindiniai rezultatai

Šiame darbe, pagal literatūroje nurodytą vėžio kamieninių ląstelių aptikimo metodiką, buvo ištirtos krūties, kasos, kiaušidžių vėžio ir melanomos ląstelių savybės. Buvo rasti minėtų ląstelių paviršiaus žymenų ekspresijos skirtumai, jautrumo chemoterapiniams vaistams ir jonizuojančiai spinduliuotei skirtumai. Taip pat skyrėsi

ląstelių gebėjimai formuoti navikus imunodeficitinėse pelėse ir atstatyti prieš rūšiavimą buvusią fenotipinę sudėtį. Nepaisant šių ląstelių skirtumų, kvantiniai taškai kaupėsi beveik vienodai visose ląstelėse. Toks rezultatas rodo, kad kvantiniai taškai galbūt geba įveikti vėžio kamieninėms ląstelėms būdingą daugiavaistinį atsparumą.

Pastaruoju metu vis dažniau mokslinėje literatūroje aptinkama duomenų apie nanodarinius, kurie selektyviai pažymėtų vėžines ląsteles ir jas sunaikintų, tačiau trūksta žinių apie tokių nanodarinių kaupimąsi ir lokalizaciją ląstelėse. Šiame darbe buvo įvertintas kvantinių taškų, kaip galimų diagnostiką ir terapiją atliekančių nanodarinių, kaupimosi ir lokalizacijos ląstelėse tyrimai. Buvo parodyta, jog antikūnais prieš paviršiaus antigeną CD44 padengti kvantiniai taškai selektyviai kaupiasi tik $CD44^+$ fenotipo ląstelėse. Nors CD44 molekulė yra paviršinė, tačiau kvantiniai taškai laikui bėgant pateko į ląstelių vidų, išsidėstė pūslelinėse struktūrose. Ateityje atradus selektyvesnę vėžinėms kamieninėms ląstelėms būdingą membranos molekulę, būtų galima sukonstruoti prieš ją antikūną ir tikėtis, jog kvantiniai taškai, padengti tokiais antikūnais, taip pat pateks į vėžinių ląstelių vidų.

Kvantinio taško ir antikūno nanodarinys atrodo daug žadantis, tačiau tinkamas tik vėžinių ląstelių atpažinimui ir vaizdinimui. Norint atlikti vėžio terapiją, reikalinga papildoma molekulė, kuri inicijuotų vėžinių ląstelių žūtį. Šiame darbe buvo ištirta kvantinio taško ir, fotodinaminėje terapijoje naudojamo, sensibilizatoriaus chlorino e_6 nanodarinio kaupimasis vėžinėse ląstelėse ir atsakas į fotosensibilizacinį poveikį. Parodyta, jog toks nanodarinys lokalizuojasi pūslelėse ląstelių viduje ir sukelia tik tų ląstelių žūtį, kurioms pritaikytas apjungtas KT-Ce_6 komplekso ir 470 nm spinduliuotės poveikis. Tokie rezultatai papildo prieš tai aptartus kvantinio taško padengto CD44 antikūnais kaupimosi ląstelėse rezultatus, parodo, jog galima kvantinį tašką ne tik selektyviai nukreipti į norimas ląsteles, bet taip pat ir įnešti į jų vidų norimą terapinę molekulę.

Kvantinio taško ir chlorino e_6 komplekso formavimasis bei kaupimasis ląstelėse buvo atliktas fiziologiniuose druskų tirpaluose, tačiau siekiant tęsti komplekso kaupimosi ir poveikio tyrimus *in vivo* sistemoje, buvo nuspręsta patikrinti, ar nanodarinio patalpinimas į baltymais ir vitaminais prisotintą mitybinę ląstelių terpę nepaveiks komplekso stabilumo. Rezultatai atskleidė, jog baltymai ir kiti terpės

komponentai neišardo hidrofobinės sąveikos rišamo komplekso. Priešingai, KT-Ce_6 kompleksas, inkubuojant baltymais ir vitaminais prisotintoje terpėje, buvo stabilesnis, nei inkubacijos metu naudojant fiziologinį druskų tirpalą. Tai tik pirminiai rezultatai, atlikti modelinėje kraujotaką primenančioje sistemoje. Tačiau tokie rezultatai padrąsina tolimesniems KT-Ce_6 komplekso kaupimosi ir pasiskirstymo tyrimams sudėtingoje *in vivo* sistemoje.

Išvados

1) Tėkmės citometrijos metodika parodyta, jog melanomos ląstelių FEMX-I $CD44^{daug}CD133^{mažai/-}$ subpopuliacija geba atkurti pradinę, prieš rūšiavimą buvusią, sudėtį ir yra mažiau jautri jonizuojančiai spinduliuotei, dėl to gali būti naudojama kaip vėžinių kamieninių ląstelių modelis priešvėžinių preparatų tyrimuose.

2) Vėžinės ląstelės, kurios yra skirtingos pagal jautrumą chemoterapiniam vaistui bei jonizuojančiai spinduliuotei, paviršinių baltymų raišką, pagal gebėjimą diferencijuotis ir formuoti navikus *in vivo,* panašiais dėsningumais kaupia CdTe-MPA ir CdSe/ZnS-(AMP)-COOH kvantinius taškus: kvantiniai taškai patenka į ląstelių citoplazmą, išsidėsto pūslelinėse struktūrose aplink branduolį, o didinant KT koncentraciją, matomas didesnis KT fotoliuminescencijos intensyvumas ląstelėse.

3) CdSe/ZnS-(AMP)-COOH KT yra intensyviau švytintys ir mažiau toksiški ląstelėms nei ZnS ir amfifilinio dangalo neturintys CdTe-MPA KT, dėl to yra tinkamesni vėžinių ląstelių vaizdinimui ir sekimui.

4) CdSe/ZnS-(AML/PEG)-COOH kvantiniai taškai, konjuguoti su antikūnu prieš vėžinių kamieninių ląstelių antigeną CD44, selektyviai jungiasi tik prie $CD44^+$ ląstelių ir yra įtraukiami į citoplazmą, priešingai nei organiniu dažu FITC žymėti analogiški antikūnai. Tai iš dalies rodo anti-CD44-KT nanodarinio gebėjimą įnešti prijungtą „krovinį“ selektyviai tik į taikiniu pasirinktų ląstelių vidų.

5) Lazerine skenuojančia konfokaline mikroskopija su spektriniu ir gyvavimo trukmių vaizdinimo priedu parodyta, jog CdSe/ZnS-(AML/PEG)-COOH KT ir sensibilizatoriaus chlorino e_6 kompleksas per 3 valandas susikaupia vėžinių ląstelių membranoje ir endocitinėse pūslelėse, neprarasdamas gebėjimo perduoti sugertos šviesos energiją iš KT į Ce_6 molekules. Komplekso lokalizacija ląstelėse, stabilumas ir energijos

pernašos efektyvumas yra pakankami, jog būtų sukelta fotosensibilizacinių vyksmų nulemta vėžinių ląstelių žūtis. Tai rodo KT gebėjimą aktyvuoti prie jo prikabintą terapinį agentą ir tokiu būdu atlikti ne tik vaizdinimo, bet ir terapijos funkciją.

6) FL gyvavimo trukmių matavimai atskleidė, jog nekovalentiškai sujungtas CdSe/ZnS-(AML/PEG)-COOH KT ir Ce_6 nanodarinys yra stabilesnis ląstelėse, kai inkubacija atliekama baltymais ir vitaminais prisotintoje, *in vivo* sistemą primenančioje terpėje, nei fiziologiniame druskų tirpale. Rezultatai atrodo daug žadantys būsimuose KT-Ce_6 komplekso tyrimuose, kurių metu bus įvertinamas jų diagnostinis ir terapinis potencialas *in vivo* aplinkoje.

6. ACKNOWLEDGEMENT

I would like to thank my supervisor prof. habil. dr. Ricardas Rotomskis for the valuable discussions, advices and support during the doctoral studies.

I thank Danute Bulotiene for her kind assistance working with experimenal animals.

I am grateful to Imunology Laboratory for helping me in the experiments with cells.

I would like to express special thanks to the team of Biomedical Physics Laboratory for the comprehension, precious discussions, support, advices and warm atmoshpere.

I am grateful to everyone for the opportunity to know you and learn from you.

Last, but not least I send my special thanks to my Family, relatives and friends for their patience, comprehension and support.

7. LIST OF PUBLICATIONS

***Thomson Reuters Web of Science*:**

1. S.Petrosiute, R.Purviniene, V.Pasukoniene, S.Lukoseviciute, P.Juzenas, R.Rotomskis. Characterization of cancer stem cells and their response to CdTe quantum dots. Medical Physics in Baltic States 8; Proceedings of International conference, Kaunas, 2010;8:71-76.

2. S.Steponkiene, R.Purviniene, S.Kavaliauskiene, P.Juzenas, R.Rotomskis. Quantum dots affect expression of CD133 surface antigen in melanoma cells. International Journal of Nanomedicine 2011;6:2437–2444.

3. A.Mlynska, V.Pašukonienė, R.Purvinienė, S.Steponkienė, A.Jagminas, R.Rotomskis. The effect of superparamagnetic iron oxide nanoparticles (SPION) on human pancreatic and ovarian cancer cells. Proceedings of International Conference "Medical Physics in the Baltic States". Kaunas, Lithuania. 2012;10:31-36.

4. R.Rotomskis, J.Valanciunaite, A.Skripka, S.Steponkiene, G.Spogis, S.Bagdonas, and G.Streckyte. Complexes of funcionalized quantum dots and chlorin e(6) in photodynamic therapy. Lithuanian Journal of Physics, 2013;53(1): 57–68.

5. S.Steponkiene, A.Skripka, J.Valanciunaite, R.Rotomskis. Cellular uptake and photosensitizing properties of quantum dot-chlorin e6 complex: in vitro study. Journal of Biomedical Nanotechnology. 2014;10(4):679-686.

National and international conferences

1. S.Petrosiute, R. Purviniene, P.Juzenas, R.Rotomskis. Cancer Stem-like Cells in FEMXI Culture and Their Response to CdTe Quantum Dots. Tarptautinė studentų ir jaunųjų mokslininkų konferencija „Chemija ir Cheminė technologija, 2010, Vilniaus, Lithuania.

2. S.Petrošiūtė, R. Purvinienė, V. Pašukonienė, S. Lukoševičiūtė, P. Juzėnas, R. Rotomskis. Characterization of cancer stem cells and their response to CdTe quantum dots, International Conference "Medical Physics in the Baltic States". 14 – 16 October 2010, Kaunas, Lithuania, 71-76 p.

3. S. Petrosiute, R. Purviniene, V.Pasukoniene, R. Rotomskis. Influence of Quantum Dots on expression of cancer stem cell markers ESA and CD44 in cancer cell line. International Conference "1st Advanced Summer School on Cancer/Regeneration Interface", 20-24 June, 2011, Porto, Portugal, 54 p.

4. S. Steponkiene, S. Kavaliauskiene, P. Juzenas, R. Rotomskis. Cancer stem-like cells and their response to quantum dots. 14th European Society for Photobiology, 1-6 September, 2011,Geneva, Switzerland, 38 p.

5.J.Valanciunaite, S.Steponkiene, A.Skripka, M.Cernych, G.Streckyte, R.Rotomskis. Photosensitizing properties and accumulation in cancer cells of non-covalent quantum dot-chlorin e6 complex. 12th International Conference on Methods and Applications of Fluorescence, September 11-14, Strasbourg, France, 221 p.

6. D.Vasiliauskaitė, S.Steponkienė, R.Rotomskis. Kvantinių taškų kaupimosi ir poveikio tyrimas MiaPaCa2 ląstelėse. Lietuvos nacionalinė fizikos konferencija, Spalio 4-6 d.,2011, Vilnius, Lietuva.

7. D.Vasiliauskaite, S.Steponkiene, R.Rotomskis. Phototoxicity of CdTe quantum dots in MiaPaCa2 cancer cells. 6th International Scientific Conference „The Vital Nature Sign". 1-4 June, 2012, Kaunas, Lithuania, 137 p.

8. A.Mlynska, V.Pašukonienė, R.Purvinienė, S.Steponkienė, A.Jagminas, R.Rotomskis. The effect of superparamagnetic iron oxide nanoparticles (SPION) on human pancreatic and ovarian cancer cells. International Conference "Medical Physics in the Baltic States". 8 – 10 November 2012, Kaunas, Lithuania, 31-36 p.

9. S.Steponkiene, J.Valanciunaite, A. Skripka, R. Rotomskis. Quantum dot-chlorin e6 complex for cancer diagnostics and treatment. International Conference "Nanomedicine 2013". 11-12 April, 2013, Barcelona, Spain, 18 p.

11. Steponkiene S, Valanciunaite J, Skripka A, Rotomskis R. Confocal spectral and lifetime imaging of quantum dot-chlorin e6 complex in living cancer cells. International Multidisciplinary Microscopy Congress, October 10-13, 2013, Turkey. Abstract book, p. 73.

12. D. Dapkute, S.Steponkiene, R. Rotomskis. Selective accumulation of quantum dots in breast cancer stem cells. Open Readings, March 19-21, 2014, Vilnius, Lithuania. Abstract book 47 p.

13. S.Steponkiene, R.Purviniene, S.Kavaliauskiene, P.Juzenas, R.Rotomskis. Cancer stem cells – a potential target in development of nanotechnology-based anticancer therapies. Nanotechnology: Research and Development, May 15-16, Vilnius, Lithuania. Abstract book 32 p.

14. D. Dapkute, S.Steponkiene. Selective accumulation of quantum dots in CD44+ breast cancer cells. Nanotechnology: Research and Development, May 15-16, Vilnius, Lithuania. Abstract book 85 p.

15. S. Bagdonas, J. Valanciunaite, A. Skripka, G. Spogis, S.Steponkiene, G. Streckyte. Complexation of a nanoparticle and a photosensitizer: implications for the photosensitized therapy. Nanotechnology: Research and Development, May 15-16, Vilnius, Lithuania. Abstract book 31 p.

Other Conferences

1. Ruta Araminaite, Vitalijus Karabanovas, Marija Ger, Mindaugas Valius, Simona Steponkiene, Ricardas Rotomskis. Targeting of Quantum Dots with Adaptor Protein Nck. 12th International Conference on Methods and Applications of Fluorescence, September 11-14, Strasbourg, France, 215 p.

2. D. Sabonis, V. Poderys, S. Steponkienė, R. Rotomskis. Au - JSA nanoklasterių spektrinių savybių ir kaupimosi vėžinėse ląstelėse tyrimai. Lietuvos nacionalinė fizikos konferencija, Spalio 4-6 d.,2011, Vilnius, Lietuva, 125 p.

3. Zdanevičius J, Statkutė U, Svirskas K, Steponkienė S. GSM-900 korinio ryšio įtaisų kuriamos elektromagnetinės spinduliuotės poveikis gyviems organizmams. 40-oji Lietuvos nacionalinė fizikos konferencija; 2013 birželio 10-12; Vilnius, Lietuva., p.134 .

8. FUNDING

- Scholarship of ERASMUS practice;
- Lithuanian and European structural funds grant “Markers of cancer stem cells for diagnostics and treatment” (2010-2011);
- Lithuanian and European structural funds grant “The application of *in vitro* modulated cells for personalized therapy of cancer” (2013-2015);
- Joint project of Lithuania, Latvia and Taiwan grant “Mesenchymal stem cell and cancer stem-like cell response to nanoparticle treatment” (2014-2016);
- European structural funds grant “Aukštos kvalifikacijos specialistų, atitinkančių valstybės ir visuomenės poreikius, biomedicinos srityje rengimo tobulinimas” (2010-2013);

9. LITERATURE

1. *World Cancer Research Fund International*. 2014 2014-05-07]; Pasaulio sergančiųjų vėži 2012 metų statistika]. Available from: http://www.wcrf.org/cancer_statistics/index.php.
2. Huang, E.H., et al., Cancer stem cells: a new paradigm for understanding tumor progression and therapeutic resistance. Surgery, 2007. **141**(4): 415-9.
3. Liu, G., et al., Analysis of gene expression and chemoresistance of CD133+ cancer stem cells in glioblastoma. Mol Cancer, 2006. **5**: 67.
4. Phillips, T.M., W.H. McBride, and F. Pajonk, The response of CD24(-/low)/CD44+ breast cancer-initiating cells to radiation. J Natl Cancer Inst, 2006. **98**(24): 1777-85.
5. Malik, B. and D. Nie, Cancer stem cells and resistance to chemo and radio therapy. Front Biosci (Elite Ed), 2012. **4**: 2142-9.
6. Zhou, Q., et al., A randomized multicenter phase II clinical trial of mitoxantrone-loaded nanoparticles in the treatment of 108 patients with unresected hepatocellular carcinoma. Nanomedicine, 2009. **5**(4): 419-23.
7. Burke, A.R., et al., The resistance of breast cancer stem cells to conventional hyperthermia and their sensitivity to nanoparticle-mediated photothermal therapy. Biomaterials, 2012. **33**(10): 2961-70.
8. Wang, C.H., et al., Photothermolysis of glioblastoma stem-like cells targeted by carbon nanotubes conjugated with CD133 monoclonal antibody. Nanomedicine, 2011. **7**(1): 69-79.
9. Goldthwaite, C.A., *Are Stem Cells Involved in Cancer?*, in *Regenerative Medicine*. 2006. p. 89-95.
10. Baumann, M., M. Krause, and R. Hill, Exploring the role of cancer stem cells in radioresistance. Nat Rev Cancer, 2008. **8**(7): 545-54.
11. An, Y. and W.M. Ongkeko, ABCG2: the key to chemoresistance in cancer stem cells? Expert Opin Drug Metab Toxicol, 2009. **5**(12): 1529-42.
12. Al Dhaybi, R., et al., Expression of CD133+ cancer stem cells in childhood malignant melanoma and its correlation with metastasis. Mod Pathol, 2010. **23**(3): 376-80.

13. de Beca, F.F., et al., Cancer stem cells markers CD44, CD24 and ALDH1 in breast cancer special histological types. J Clin Pathol, 2013. **66**(3): 187-91.
14. Chen, K., Y.H. Huang, and J.L. Chen, Understanding and targeting cancer stem cells: therapeutic implications and challenges. Acta Pharmacol Sin, 2013. **34**(6): 732-40.
15. Chen, J., et al., CD133 and CD44 are universally overexpressed in GIST and do not represent cancer stem cell markers. Genes Chromosomes Cancer, 2012. **51**(2): 186-95.
16. Melancon, M.P., M. Zhou, and C. Li, Cancer theranostics with near-infrared light-activatable multimodal nanoparticles. Acc Chem Res, 2011. **44**(10): 947-56.
17. Zrazhevskiy, P., M. Sena, and X. Gao, Designing multifunctional quantum dots for bioimaging, detection, and drug delivery. Chem Soc Rev, 2010. **39**(11): 4326-54.
18. Alivisatos, A.P., W. Gu, and C. Larabell, Quantum dots as cellular probes. Annu Rev Biomed Eng, 2005. **7**: 55-76.
19. Smith, A.M., et al., Bioconjugated quantum dots for in vivo molecular and cellular imaging. Adv Drug Deliv Rev, 2008. **60**(11): 1226-40.
20. Juzenas, P., et al., Quantum dots and nanoparticles for photodynamic and radiation therapies of cancer. Adv Drug Deliv Rev, 2008. **60**(15): 1600-14.
21. Yang, K., et al., In-vivo imaging of oral squamous cell carcinoma by EGFR monoclonal antibody conjugated near-infrared quantum dots in mice. Int J Nanomedicine, 2011. **6**: 1739-45.
22. Cai, W., et al., Peptide-labeled near-infrared quantum dots for imaging tumor vasculature in living subjects. Nano Lett, 2006. **6**(4): 669-76.
23. Samia, A.C., X. Chen, and C. Burda, Semiconductor quantum dots for photodynamic therapy. J Am Chem Soc, 2003. **125**(51): 15736-7.
24. Idowu, M., J.Y. Chen, and T. Nyokong, Photoinduced energy transfer between water-soluble CdTe quantum dots and aluminium tetrasulfonated phthalocyanine. New Journal of Chemistry, 2008. **32**(2): 290-296.

25. Shi, L.X., B. Hernandez, and M. Selke, Singlet oxygen generation from water-soluble quantum dot-organic dye nanocomposites. Journal of the American Chemical Society, 2006. **128**(19): 6278-6279.
26. Fodstad O, K.I., Aamdal S, Extrapulmonary, tissue-specific metastasis formation in nude mice injected with FEMX-I human melanoma cells. Cancer Research, 1988. **48**: 4382-4388.
27. Lakowicz, J.R., *Principles of fluorescence spectroscopy*. 3rd ed. 2006, New York: Springer. xxvi, 954 p.
28. Steponkiene, S., et al., Quantum dots affect expression of CD133 surface antigen in melanoma cells. Int J Nanomedicine, 2011. **6**: 2437-44.
29. Baba, T., et al., Epigenetic regulation of CD133 and tumorigenicity of CD133+ ovarian cancer cells. Oncogene, 2009. **28**(2): 209-18.
30. Ding, Q., et al., Establishment of a highly migratory subclone reveals that CD133 contributes to migration and invasion through epithelial-mesenchymal transition in pancreatic cancer. Hum Cell, 2012. **25**(1): 1-8.
31. Gisina, A.M., et al., Subpopulation of colorectal adenocarcinoma cells co-expressing CD133 and cancer stem cells markers of other tumors. Bull Exp Biol Med, 2012. **152**(6): 739-42.
32. Liu, L., et al., In vitro and In vivo Assessment of CdTe and CdHgTe Toxicity and Clearance. J Biomed Nanotechnol, 2008. **4**(4): 524-528.
33. Lovric, J., et al., Differences in subcellular distribution and toxicity of green and red emitting CdTe quantum dots. J Mol Med (Berl), 2005. **83**(5): 377-85.
34. Cho, S.J., et al., Long-term exposure to CdTe quantum dots causes functional impairments in live cells. Langmuir, 2007. **23**(4): 1974-80.
35. Sun, D., et al., Study on effect of peptide-conjugated near-infrared fluorescent quantum dots on the clone formation, proliferation, apoptosis, and tumorigenicity ability of human buccal squamous cell carcinoma cell line BcaCD885. Int J Nanomedicine, 2010. **5**: 401-5.
36. Hoshino, A., S. Hanada, and K. Yamamoto, Toxicity of nanocrystal quantum dots: the relevance of surface modifications. Arch Toxicol, 2011. **85**(7): 707-20.

37. Yong, K.T., et al., Nanotoxicity assessment of quantum dots: from cellular to primate studies. Chem Soc Rev, 2013. **42**(3): 1236-50.
38. Muller-Borer, B.J., et al., Quantum dot labeling of mesenchymal stem cells. J Nanobiotechnology, 2007. **5**: 9.
39. Shah, B., et al., Labeling and imaging of human mesenchymal stem cells with quantum dot bioconjugates during proliferation and osteogenic differentiation in long term. Conf Proc IEEE Eng Med Biol Soc, 2006. **1**: 1470-3.
40. Damalakiene, L., et al., Intracellular distribution of nontargeted quantum dots after natural uptake and microinjection. Int J Nanomedicine, 2013. **8**: 555-68.
41. Galanzha, E.I., J.W. Kim, and V.P. Zharov, Nanotechnology-based molecular photoacoustic and photothermal flow cytometry platform for in-vivo detection and killing of circulating cancer stem cells. J Biophotonics, 2009. **2**(12): 725-35.
42. Jennings, T.L., et al., Reactive semiconductor nanocrystals for chemoselective biolabeling and multiplexed analysis. ACS Nano, 2011. **5**(7): 5579-93.
43. Valanciunaite, J., et al. *Complex of water-soluble CdSe/ZnS quantum dots and chlorin e6: interaction and FRET*. in *Laser Applications in Life Sciences*. 2010 2010. 7376.
44. Steponkiene, S., et al., Cellular uptake and photosensitizing properties of quantum dot-chlorin e6 complex: in vitro study. J Biomed Nanotechnol, 2014. **10**(4): 679-86.
45. Frolov, A.A., et al., Chlorin e6-liposome interaction. Investigation by the methods of fluorescence spectroscopy and inductive resonance energy transfer. Journal of Photochemistry and Photobiology. B, Biology, 1990. **7**(1): 43-56.
46. Mojzisova, H., et al., The pH-dependent distribution of the photosensitizer chlorin e6 among plasma proteins and membranes: a physico-chemical approach. Biochim Biophys Acta, 2007. **1768**(2): 366-74.
47. Valanciunaite, J. and R. Rotomskis, Quantum Dots as Energy Donors for Photosensitizers: Perspectives for Photodynamic Therapy of Cancer. Medical Physics in the Baltic States, 2010(2): 44-49.
48. Bechet, D., et al., Nanoparticles as vehicles for delivery of photodynamic therapy agents. Trends Biotechnol, 2008. **26**(11): 612-21.

49. Cheng, S.H. and L.W. Lo, Inorganic nanoparticles for enhanced photodynamic cancer therapy. Curr Drug Discov Technol. **8**(3): 250-68.
50. Gamaleia, N.F., et al., Photodynamic activity of hematoporphyrin conjugates with gold nanoparticles: experiments in vitro. Exp Oncol. **32**(1): 44-7.
51. Hsu, C.Y., et al., Bioluminescence resonance energy transfer using luciferase-immobilized quantum dots for self-illuminated photodynamic therapy. Biomaterials. **34**(4): 1204-12.